Research Article

For reprint orders, please contact: reprints@futuremedicine.com

Regenerative Medicine

# Selected renal cells modulate disease progression in rodent models of chronic kidney disease via NF-κB and TGF-β1 pathways

**Aim:** Identification of mechanistic pathways for selected renal cell (SRC) therapeutic bioactivity in rodent models of chronic kidney disease. **Materials & methods:** *In vivo* and *in vitro* functional bioassays applied to investigate regenerative outcomes associated with delivery of SRC to diseased rodent kidney. **Results:** *In vivo*, SRC reduces chronic infiltration by monocytes/macrophages. SRC attenuates NF-κB and PAI-1 responses while simultaneously promoting host tubular cell expansion through trophic cues. *In vitro*, SRC-derived conditioned media attenuates TNF-α-induced NF-κB response, TGF-β-mediated PAI-1 response and increases expression of transcripts associated with cell cycle regulation. Observed bioactive responses were from vesicle and nonvesicle-associated factors, including specific miRNAs. **Conclusion:** We identify a paracrine mechanism for SRC immunomodulatory and trophic cues on host renal tissues, catalyzing long-term functional benefits *in vivo*.

**Keywords:** cell therapy • chronic kidney disease • fibrosis • inflammation • mechanism of action • miRNA • NF-κB • PAI-1 • paracrine • regeneration • selected renal cell • stem cell • tissue engineering • vesicle

Andrew T Bruce[1,2], Roger M Ilagan[1,2], Kelly I Guthrie[1,2], Elias Rivera[2,3], Sumana Choudhury[2,4], Namrata Sangha[2,5], Thomas Spencer[2,6], Timothy A Bertram[2,6], Deepak Jain[2,6], Russell W Kelley[2,7] & Joydeep Basu*[,2,6]

[1]Regenerative Medicine, United Therapeutics, 55 TW Alexander Drive, Research Triangle Park, NC 27709, USA
[2]Tengion, Inc., 3929 Westpoint Blvd, Ste G, Winston-Salem, NC 27103, USA
[3]Infinium Pathology Consultants LLC, 1805 Wild Fern Dr., Oak Ridge, NC 27310, USA
[4]Gene Therapy Center, Vector Core, University of North Carolina at Chapel Hill, NC 27617, USA
[5]Wake Forest Institute for Regenerative Medicine, Medical Centre Boulevard, Winston-Salem, NC 27157, USA
[6]RegenMedTX LLC, 3929 Westpoint Blvd, Ste G, Winston-Salem, NC 27103, USA
[7]Burroughs Wellcome Fund, 21 TW Alexander Drive, Research Triangle Park, NC 27709, USA
*Author for correspondence:
Tel.: +1 336 722 5855
Fax: +1 336 722 2436
jbasu2@yahoo.com

Chronic kidney disease (CKD) represents a significant and increasing healthcare issue in North America and the rest of the world. Observed rates of increase are due principally to development of renal failure secondary to noninsulin-dependent diabetes and hypertension [1]. Modern strategies for management of the CKD patient population are based on pharmaceuticals for amelioration of the primary disease (i.e., glycemic control agents and antihypertensive agents) that serve to modulate development of secondary renal damage and disease. Ultimately, however, dialysis or whole organ transplantation is indicated as a proxy for renal filtration functionality. Patients presenting with advanced CKD are also controlled through pharmaceuticals to restore other key aspects of renal bioactivity, including erythropoiesis catalyzed by erythropoietin (EPO), and secretion of vitamin D from tubule-specific vitamin D hydroxylase [2]. Whole kidney transplantation remains the standard of care, but the CKD patient population advancing to end-stage renal disease (ESRD) requiring dialysis or transplant is much greater than the number of acceptable donor kidneys [3]. To this end, regenerative medicine and tissue-engineering methodologies may provide additional therapeutic possibilities for CKD patients.

Rescue of renal functionality with cell-based methodologies has been explored clinically for acute renal failure (ARF) with extracorporeal filtration units containing renal tubular cells [4], and by transfer of allogeneically sourced mesenchymal stem cells (MSCs) through the renal artery [5,6]. These approaches mediate short-term recovery of defined renal functionalities. Preclinical studies involving delivery of different cell populations immediately before or after establishment of ARF include: intrarenal or systemic delivery of MSC [7], fetal cells or tissue rudiments [8–11] and endothelial progenitor cells (EPC) [12,13]. Preclinical studies of cell-based therapies for CKD are limited, with few sys-

Future Medicine part of fsg

tematic investigations of the therapeutic potential of cell-based treatments after onset of chronic injury. Therapeutic bioactivity has been observed in rodent models of Alport syndrome following treatment with bone marrow cells [14], in rodent models of partial nephrectomy or ischemia-reperfusion injury following systemic injection with fetal kidney cells [15], and in swine models of unilateral renal artery stenosis following treatment with autologously sourced EPC [13].

Typically, strategies currently under consideration for cell therapy of the kidney in response to onset of CKD have focused on leveraging the potential paracrine-mediated therapeutic properties of MSC, embryonic stem cells and related cell populations (reviewed by [16]). However, from a manufacturing and product development perspective, primary cell types are preferable when compared with stem and progenitor cell populations, owing to considerable streamlining of isolation, expansion, maintenance and characterization conditions (reviewed by [17,18]). To this end, numerous studies on regeneration of renal architecture and function following acute kidney injury point to tubular epithelial cells as central in restoration of renal functionality [19,20].

Tubular cells can be separated from other kidney cell types on the basis of differential buoyant density [21]. This predominant population of tubular cells is reproducibly separable from remnant cells as a well-defined band (B2) with buoyant density between 1.045 and 1.063 g/ml and is characterized as an epithelial cell-enriched population comprised of tubular and aquaporin 2-positive collecting duct cells [21]. Upon delivery to 5/6-nephrectomized (5/6$N_x$) rats 4–7 weeks postinjury, B2 cells stimulated tissue regeneration and stabilized renal filtration functions for 6 months post-treatment, leading to 100% survival in treated rats versus 0% survival in untreated rats. B2 cells were therefore leveraged to form the principal component of selected renal cells (SRCs; see the 'Materials & methods' section for additional details). B1 and B5 cell populations, representing additional defined bands with distinct buoyant densities, were observed to be therapeutically inert in rodent CKD models, and are additionally leveraged as non-SRC cellular controls in the current report [21–23]. These cell populations (B1–B5) have been phenotypically characterized in detail at the morphological, transcriptomic and immunohistochemical (IHC) levels [21–23] and are composed of principally E-cadherin (ECAD$^+$), Pan-cadherin$^+$, cytokeratin 8/18/19 (CK8/18/19$^+$), gamma glutamyl transpeptidase (GGT1$^+$) cells and oxygen responsive EPO$^+$ (erythropoietin) subpopulations [21–23].

From a mechanism of action (MOA) perspective, although engraftment of SRC within the treated kidney has been demonstrated out to 6 months postimplantation [21–23], this is likely not the only therapeutic mechanism at play for preserving nephron function and delaying overt tissue inflammation and fibrosis. The ability to augment renal function with SRC might reflect a combination of the potential of the engrafted cell to salvage cellular compartments and the autocrine, paracrine and perhaps endocrine factors that are transiently and/or constitutively transferred to a recipient diseased cell from the donor cell population. Additionally, we note that SRC have not been observed to engraft at sites other than the targeted kidney.

The development of tubulointerstitial fibrosis during the progression of CKD is associated with TGF-β1-mediated epithelial–mesenchymal transition (EMT) of tubular epithelial cells [24]. Progressive fibrosis is a hallmark of CKD and is a clear feature of the 5/6$N_x$ model. The accumulation of fibrotic extracellular matrix (ECM) proteins, which include fibronectin (FN) and type I collagen, has long been associated with persistent expression of TGF-β1 by injured or distressed cells [25]. Plasmin-dependent proteolysis of ECM proteins, through the increased expression of PAI-1, can further promote the development of fibrotic lesions [26]. It has been demonstrated that TGF-β1 and PAI-1 interact within a positive feedback loop that may, in the absence of intervention, trigger pathologies associated with uncontrolled deposition and inadequate degradation of ECM [27]. Molecular analyses of diseased rodent kidney tissue at the time of necropsy (3 and 6 months after treatment) demonstrate that treatment with B2 attenuated expression of TGF-β1, PAI-1 and FN [21–23]. These observations taken together suggest that B2 cells are communicating to host cells through paracrine factors. This hypothesis is supported, in part, by the observation that the reduction in profibrotic markers is maintained even 6 months after implantation, despite the relatively low number of donor cells as detected by PCR-based analysis of *SRY* in those same tissues [21–23].

In this manuscript, we extend our previously published observations by hypothesizing a paracrine-mediated MOA for observed therapeutic bioactivity of SRC in preclinical rodent models of CKD (5/6$N_x$ Lewis rats and ZSF1 diabetic nephropathy model, see the 'Materials & methods' section below). Specific histological observations of antifibrotic and anti-inflammatory outcomes secondary to SRC delivery in rodent CKD kidneys led us to investigate at a molecular level the NF-κB and TGF-β1-mediated PAI-1 signaling pathways known to drive tissue inflammation and fibrosis during onset of CKD [27]. We further hypothesize that these SRC-derived paracrine factors may function through extracellular vesicle-mediated communication mechanisms. To this end, we used molecular histologic techniques to show SRC can attenuate the NF-κB and PAI-1 responses known to drive tissue

inflammation and fibrosis, while simultaneously promoting host tubular cell expansion through trophic cues. As an indicator of renal-specific and NF-κB-mediated inflammatory status, urine CCL2/MCP-1 and CCL5/RANTES protein levels were measured by ELISA [28] and observed to at least partially be modulated in response to SRC. Consistent with these *in vivo* outcomes, we demonstrate that SRC-derived conditioned media (CM) can attenuate the TNF-α-induced NF-κB response, TGF-β1-mediated PAI-1 response and increase expression of transcripts associated with cell cycle regulation in established renal cell lines. Observed bioactive responses were from vesicle and nonvesicle-associated factors present in SRC-CM. These *in vitro* findings recapitulate our *in vivo* analysis of rat SRC-treated kidneys: robust inhibition of NF-κB activation and PAI-1 expression and increased number of proliferative cells in targeted tissues is observed following direct SRC injection. Taken together, these data identify a paracrine mechanism by which SRC may provide immunomodulatory and trophic cues to diseased host renal tissues.

## Materials & methods

### Animal models of CKD

Materials generated from rodent models of CKD were derived from studies previously described [21–23,29]. For characterizing the pathogenesis of CKD, 30 female Lewis rats underwent a two-step 5/6$N_x$ procedure as previously described [29]. ZSF1 rats were provided by Charles Rivers Laboratories and are a hybrid strain generated from the zucker diabetic fatty rat (ZDF-1; *Lepr*$^{+/fa}$) and the spontaneously hypertensive heart failure rat (SHHF/Mcc, *Lepr*$^{+/cp}$). The ZSF1 rat strain provides an experimental model for translating the potential utility of cell-based therapies for preventing or delaying renal disease progression secondary to Type 2 diabetes. The metabolic syndrome and the progressive diabetic nephropathy (DN) in the ZSF1 culminate from morbid obesity, severe hyperglycemia, hyperinsulemia and hyperlipidemia, hypertension and cardiovascular complications that also increase the risk of congestive heart failure [30,31]. An overview of study design is presented in Tables 1 & 2. Clinical parameters associated with entry criteria and evaluation of therapeutic outcomes are described in detail in [21–23,29] and will not be repeated here. While the ZSF1 model may survive up to 63 weeks of age, a more typical survival time is 48 weeks of age [30,31]. Within the first 8 weeks of life, ZSF1 rats present with the hallmark indicators of metabolic syndrome which includes Type 2 diabetes and initial signs of renal functional impairment, and by 32 weeks of age, ZSF1 kidney structure and function have declined significantly and are consistent with

Table 1. Summary of Lewis 5/6$N_x$ experimental design.

| 1 week | | 4–7 weeks | | 8–24 weeks | Ref. |
|---|---|---|---|---|---|
| **Model generation two-step 5/6$N_x$** | **Establishment of disease state** | **Entry into study** | **Treatment** | **Clinical outcomes** | |
| Day 0, left kidney 2 poles removed<br>Day 7, right kidney removed | sCREAT and BUN monitored weekly standard chow/water *ad libitum* | Criteria: ↑ sCREAT ≥200% ↑ BUN >200% >2 consecutive weeks | Randomization | Slowed progression by improving functional renal mass; 6-month survival | [22] |

Test:
– Intrarenal delivery of 5 × $10^6$ SRC (B2 + B4 cells) delivered to cortex of remnant kidney (n = 3)
Controls:
– Intra-renal delivery of 5 × $10^6$ non-SRC (B1 + B5 cells) delivered to cortex of remnant kidney (n = 2)
– Nephrectomy (n = 3)
– Hemi-nephrectomy (n = 3)

BUN: Blood Urea Nitrogen; sCREAT: Serum creatinine; SRC: Selected renal cell.

Table 2. Summary of ZSF1 experimental design.

| 1–17 weeks | | | 18 weeks | | 31 weeks | 32–63 weeks | Ref. |
|---|---|---|---|---|---|---|---|
| Establishment of disease state | Entry into study | Treatment | | | | Clinical outcomes | |
| Metabolic syndrome of obesity, diabetes mellitus, hypertension; fed diabetogenic diet | Criteria: 65% functional eGFR | Randomization | Test:<br>– Intraparenchymal delivery of 2.5 × $10^6$ SRC in 100 µl volume in each of the anterior and posterior poles of both kidneys (n = 7)<br>Controls:<br>– Obese no treatment (n = 5)<br>– Lean no treatment (n = 5) | Diet changed to maintenance diet plus insulin | | Improved nephron function by increasing filtration ↓ sCre and BUN, increased tubular transport ↓ sCal sPhos and improved ability to concentrate urine ↑ uOsmol; improved survival | [23] |

SRC: Selected renal cell; eGFR: Estimated glomerular filtration rates; sCre: Serum Creatinine; sCal: Serum calcium; sPhos: Serum phosphate; uOsmol:Urine osmolality.

DN [30,31]. By 18 weeks of age, ZSF1 renal function is significantly impaired under the study conditions described herein. Using defined estimated glomerular filtration rate (eGFR) staging criteria, ZSF1 rats possessed approximately 65% remaining eGFR function at the time of SRC implant. We measured survival of the ZSF1 rats under the conditions described herein up to 63 weeks of age (45 weeks on study). Only one of five untreated ZSF1 rats survived the study (80% mortality) compared with six of seven surviving animals in the treated group (1/7; <15% mortality). All of the lean animals were alive at the end of study. See [23] for additional details. Our attempts to intervene at a later time point (more chronic model) have been complicated by poor survival rates of these notably sicker animals following surgery. 18 weeks of age represents a reasonable compromise between development of clinically relevant disease criteria while maintaining acceptable survival outcomes postsurgery. Ethical considerations pertinent to the treatment of all research animals used in this study were evaluated by the Institutional Animal Care and Use Committee (IACUC) at the site of this research.

### SRC renal cell culture & transplantation

The preparation of selected bioactive primary renal cells from whole rat kidney has been previously described in detail [21–23,29]. Briefly, whole kidneys were harvested from 5-week-old male Lewis rats (Hilltop Labs, PA, USA) and kidney tissue was dissociated enzymatically in a buffer containing 4.0 units/ml dispase (Stem Cell Technologies, Inc., BC, Canada) and 300 units/ml collagenase IV (Worthington Biochemical, NJ, USA). Red blood cells and debris were removed by centrifugation through 15% iodixanol (Optiprep®, Axis Shield, MA, USA). Primary renal cells were seeded onto tissue culture-treated polystyrene plates (NUNC, NY, USA) and cultured in 50:50 media, a 1:1 mixture of high glucose Dulbecco's Modified Eagle Medium (DMEM):keratinocyte serum-free medium (KSFM) containing 5% fetal bovine serum, 2.5 µg EGF, 25 mg bovine pituitary extract, 1× ITS (insulin/transferrin/sodium selenite medium supplement) and antibiotic/antimycotic (all from Invitrogen, CA, USA). Prior to postculture cell separation, primary renal cell cultures were transferred from atmospheric oxygen conditions (21%) to a more physiologically relevant low-oxygen (2%) environment for 24 h, to improve cell separation efficiency. Separation of primary renal cell cultures, prepared as 75 × $10^6$ cells in 2 ml unsupplemented KSFM (uKSFM), was performed by centrifugation through a four-step iodixanol (OptiPrep; 60% w/v in uKSFM) density gradient-layered specifically for rodent (16, 13, 11 and 7%) in 15 ml conical polypropylene tubes and

Table 3. Renal biomarker profiles for 5/6 nephrectomized rodent models of chronic kidney disease treated with selected renal cells at 12 weeks on study.

| Clinical biomarker (12 weeks post-$T_x$) | Sham nephrectomy (n = 5) | Nephrectomy (5/6) (n = 8) | SRC treatment (n = 3) | p-value |
|---|---|---|---|---|
| **Glomerular function** | | | | |
| Serum creatinine (mg/dl) | 0.4 ± 0.0 | 1.13 ± 0.15 | 0.70 ± 0.10 | $p < 0.01$ and $p \geq 0.001$ |
| BUN (mg/dl) | 18.0 ± 1.41 | 45.71 ± 5.41 | 36.33 ± 7.77 | $p < 0.05$ and $p \geq 0.01$ |
| **Tubular function** | | | | |
| Serum albumin (g/dl) | 4.22 ± 0.08 | 2.84 ± 0.10 | 3.30 ± 0.10 | $p < 0.001$ |
| A:G ratio (A/G) | 1.19 ± 0.04 | 0.80 ± 0.04 | 1.05 ± 0.12 | $p < 0.01$ and $p \geq 0.001$ |

Means ± standard deviation, see also [22].
BUN: Blood urea nitrogen; SRC: Selected renal cell; $T_x$: treatment.

centrifuged at 800 g for 20 min at room temperature (without brake). After centrifugation, cellular subfractions were extracted from the gradient via pipette and collected as four distinct bands (B1–B4) and a pellet (B5). All bands were washed three-times with sterile phosphate buffered saline prior to use. Therapeutically bioactive renal cells were produced by combining B2 and band 4 (B4) from the density gradient centrifugation step at a ratio of 97% B2 to 3% B4. This results in a population of tubular cell-enriched cells previously demonstrated to significantly stabilize serum creatinine and blood urea nitrogen (BUN) and improve survival in the rodent 2-step 5/6$N_x$ of CKD [21–23]. B1/B5 has been previously demonstrated to be therapeutically inert and functioned as a non-SRC cellular control [21–23]. B1 cells are predominantly distal tubular and collecting duct cells with trace amounts of other cell types. B5 contains vascular, endocrine and glomerular cells [21–23]. Recipient female Lewis 5/6$N_x$ rats or male ZSF1 obese rats (all from Charles Rivers Laboratories) were anesthetized, and the kidneys for treatment were exposed by a ventral medial-lateral incision. Cell suspensions (100 µl) were loaded into a 1 cc syringe fitted with a half inch 23G needle (Becton Dickinson, RTP, NC, USA) and injected directly into the kidney parenchyma at a depth of 3–5 mm as previously described [21–23,29]. 5/6$N_x$ Lewis rats received a single dose into the remnant kidney, while ZSF1 obese rats received four doses, one at each pole of each kidney.

## SRC product potency

Assays for SRC product potency were based on functional characterization of B2-associated glutamyl transpeptidase (GGT1) activity and megalin:cubilin-mediated albumin transport as described in [22]. Specificity of albumin transport was demonstrated by blockage with RAP, a known competitive inhibitor of megalin:cubilin-mediated albumin uptake, and by absence of transport in the nontubular B4 subpopulation as described in [22].

## Conditioned media

CM was derived from cultures of human SRC collected and centrifuged at 3500 g for 30 min at 4°C to remove debris and supernatant collected. To identify bioactive components, CM was subjected to ultracentrifugation at 200,000 g for 2 h at 4°C. The ultracentrifuge pellet (containing secreted vesicles) was resuspended in basal media (DMEM:KSFM alone) at 1/5 of the original volume. Supernatant media (here termed vesicle-free media [VFM]) was collected and further fractionated using Viva-spin™ semipermeable polyethersulfone membrane concentrators (GE Healthcare, NY, USA) with molecular weight cutoffs (MWCO) at 5, 10, 50 and 100 kDa.

## Cell culture experiments & transfections

The human proximal tubule cell line, HK2 (ATCC) was maintained in 1:1 mixture of high glucose DMEM and KSFM containing 5% (v/v) fetal bovine serum, 2.5 µg EGF, 25 mg bovine pituitary extract, 1× ITS (insulin/transferrin/sodium selenite medium supplement) and 1× antibiotic/antimycotic (all from Life Technologies). HK2 cells were transfected using NF-κB reporter plasmid construct, pGL4.32[*luc2P*/NF-κB-RE/Hygro] (Promega, WI, USA) using Lipofectamine™-2000 transfection reagent (Life Technologies) and single clonal colonies subcultured through several passages in selective growth media containing 100 µg/ml Hygromycin B (Life Technologies) to generate a stable cell line. Transcriptional activation of the NF-κB reporter was determined using ONE-Glo™ luciferase reagent (Promega). For proliferation experiments, near-confluent

Table 4. Renal biomarker profiles for ZSF1 obese rats treated with selected renal cells at 16 or 24 weeks post-treatment, as percentage of baseline.

| Clinical biomarker (16 or 24 weeks post-$T_x$) | ZSF (obese; n = 5) | ZSF (obese) + SRC (n = 5) | p-value |
|---|---|---|---|
| **Glomerular function** | | | |
| Serum creatinine (μmol/l) | 53 ± 2.7 | 44.2 ± 1.8 | 0.014 |
| BUN (mmol/l) | 11.42 ± 0.75 | 8.21 ± 0.61 | 0.029 |
| **Tubular function** | | | |
| Calcium (mmol/l) | 3.02 ± 0.04 | 2.87 ± 0.03 | 0.020 |
| Phosphorus (mmol/l) | 2.23 ± 0.08 | 1.97 ± 0.06 | 0.030 |
| **Loop of Henle and collecting duct** | | | |
| Urine osmolality (mOsmol/kg) | 681 ± 48.7 | 901 ± 41.6 | 0.007 |
| Urine specific gravity | 1.034 ± 0.001 | 1.040 ± 0.001 | 0.001 |

See also [23].
BUN: Blood urea nitrogen; SRC: Selected renal cell.

monolayers of HK2 cells were serum starved in basal media (DMEM:KSFM) for 2 h prior to 24- and 48-h exposures to SRC-CM. CM was prepared as described above. CM was collected from rat and human cultures of SRC under serum- and supplement-free conditions and utilized for *in vitro* assays. Commercially available human-derived renal mesangial cells (HRMC) were used as surrogates for host-response tissues in the *in vitro* assays since mesangial cells express PAI-1 in injured/diseased kidneys. Vesicular particles shed by cells into the culture media were collected by high-speed centrifugation and total RNA was extracted from the pellet with TRIzol reagent (Invitrogen, CA, USA). RNA content of vesicles was screened using PCR-based arrays of known miRNA sequences with a focus on miRNAs known to be involved in fibrosis and inflammation (Qiagen, CA, USA). miRNA was synthesized (Invitrogen) for transfection using Lipofectamine-2000 according to manufacturer's instructions.

## Quantitative RT-PCR

Total RNA was extracted from cells and tissues using the RNeasy-Plus Mini Kit/QIA-shredder (Qiagen). cDNA was synthesized from 700 ng total RNA using SuperScript® VILO™ cDNA Synthesis Kit (Life Technologies). Gene amplification was performed with ABI-Prism 7300 real-time PCR system using the following TaqMan® primer/probe sets (Life Technologies): rat *CCL5* (Rn00579590_m1), rat *CD68* (Rn01495634_g1), rat *CD3* (Rn01417940_m1), rat *PPIB* (Rn00574762_m1), rat Serpine (Rn00561717_ml), human *CCND1* (Hs00765553_m1), human *FOS* (Hs00170630_m1), human *PPIA* (Hs99999904_m1). Relative gene-expression was calculated using comparative cycle threshold (ΔΔCt) method with *PPIB* (rat tissues) or *PPIA* (human cells) as endogenous control. Values were calibrated to experimental controls (e.g., unmanipulated rats, unilateral $N_x$ rats, basal media-treated cells).

## Western blot

Kidney tissues were snap-frozen in liquid nitrogen and homogenized using mortar and pestle prior to lysis. Cell culture samples were processed directly without snap freezing. Nuclear and cytoplasmic fractions were isolated using the NE-PER extraction kit following manufacturer's protocol (Thermo Fisher Scientific, MA, USA). Western blotting was performed as described in [29]. Membranes were probed overnight at 4°C in 2% (w/v) nonfat milk in TBST with the following antibodies: 1:5000 anti-βActin (A5441, Sigma-Aldrich, MO, USA), 1:500 anti-IκBα (ab32518, Abcam, MA, USA), 1:250 anti-CD3 (ab5690, Abcam), 1:500 anti-CD68 (ab31630, Abcam), 1:250 anti-PTEN (ab32199, Abcam), 1:1000 anti-PCNA (ab29, Abcam), 1:500 anti-p65 (ab7970, Abcam), 1:20 anti-PAI-1 (612025 BD), 1:40 anti-FN (MAB1918, R&D), 1:1000 anti-p50 (ab32360, Abcam), 1:200 anti-Lamin B1 (ab16048, Abcam). For each western blot, n = 3 independent experiments were performed, with n = 3 replicates per protein of interest. Quantitation of western blots was performed with NIH Image J software [32].

## Enzyme-linked immunosorbent assays

Protein concentration of kidney tissue lysates was determined by Bradford assay and normalized to final concentration of 25 μg/ml. Urine samples were diluted 1:200 for CCL2/MCP–1 and 1:1.5 for CCL5/RANTES. CCL2 and CCL5 concentrations were determined by ELISA following manufacturer's instructions (Ray-Biotech, GA, USA). Absorbance at 450 nm was determined on the FLUO-star Omega microplate reader (BMG Labtech, Offenburg, Germany).

### Immunohistochemistry

Rat kidneys were fixed in formalin, processed for paraffin embedding, sectioned and stained by immunohistochemistry following standard protocols (Premier Labs, CO, USA). Primary antibodies used for immunohistochemistry were: anti-p65 (ab7970, Abcam), anti-CD3 (A0452, Dako, CA, USA), anti-CD68 (MCA341R, AbD Serotec) and anti-Ki67 (M7248, Dako). Quantitative image analysis was performed on anti-p65 (ab7970, Abcam) and anti-PAI-1 (ab28207, Abcam) stained sections from SRC-treated and untreated 5/6$N_x$ and ZSF1 obese rats at end of study following standard protocols with Scanscope XT (Aperio, IL, USA), completed slides were scanned into digital images (apparent magnification 20×). Image analysis was performed with modified version of Aperio's positive pixel count algorithm (Premier Labs).

### Immunofluorescence & image analysis

Cell immunofluorescence was as previously described [22,23]. Quantification of NF-κB bioactivity was based on scoring the number of positive nuclei. Image quantification was performed using IN Cell Analyzer, Multi-Target Analysis (MTA) software (GE Healthcare).

### Statistical analysis

For gene- and protein-expression data in rat tissues/human cells, data are presented as average of three animals/replicates (except n = 2 for cell treatment group), with standard error of mean calculated for each group. Statistical significances between experimental groups were determined by unpaired, two-tailed student's *t*-tests. For urinary cytokine expression (CCL2, CCL5), multivariate models were constructed with JMP version 7.0 software (SAS Institute, NC, USA) to determine statistical significance of treatment effects. Effect of SRC-CM on translocation of NF-κB was tested using logistic regression analysis with JMP version 7.0 software (SAS Institute). Chi-square analyses were performed comparing the frequency of the 'high' and total ('high' + 'low') activation in basal media versus SRC-CM, with and without TNF-α stimulation.

## Results

### SRC product potency

Functional assays confirmed that the observed expression of GGT1 and cubilin resulted in active proteins [22]. Nitroaniline was produced by active GGT1 in B2 cells, and fluorescently tagged albumin was actively transported into cubilin-positive B2 cells [22]. Taken together, these data confirm SRC product potency prior to *in vivo* cell transplantation studies.

### Progressive NF-κB activation & interstitial inflammation are features in the development of CKD in the 5/6 nephrectomy model

To understand the temporal dynamics of the 5/6$N_x$ model of CKD and to evaluate involvement of NF-κB signaling in disease progression, we conducted a time-course analysis of 5/6$N_x$ Lewis rats and assayed kidney tissue at 1, 2, 4, 6 and 8 weeks postsurgery. Unmanipulated control kidneys were collected at the beginning of the study. We observed a time-dependent increase in both expression and nuclear localization of NF-κB p65 subunit, particularly during the chronic phase of disease progression (2–8 weeks postnephrectomy), see histological outcomes summarized in Table 4.

In histological sections of remnant kidneys, few cells showed evidence of nuclear p65 at 2 weeks postnephrectomy; however, increase of cytoplasmic (inactive) p65 in distal tubular cells was observed (Figure 1A). At 6 weeks post-nephrectomy, robust p65 nuclear localization was observed in tubular epithelial cells and glomerular cells (Figure 1A). Significantly higher expression of p65 was observed in glomerular cells of 5/6$N_x$ rats compared with the tubular compartment (Figure 1A). Increased NF-κB activity was confirmed semiquantitatively by p65 western blot analysis on cytoplasmic and nuclear extracts taken at selected time points during the 8-week study (Figure 1E). Data were quantified by calculating the ratio: intensity p65 (nucleus)/intensity p65 (cytoplasm) relative to the control sample (set as 1). As shown in Figure 1E, this ratio increased to 6.7 at 1-week postnephrectomy and increased further to 9.4 by 6-week postnephrectomy, confirming a significant transfer of cytoplasmic p65 to the nucleus in response to injury.

Beginning at the 2-week time point, *CCL5* gene-expression was increased four- to six-fold over unmanipulated controls and these levels were maintained throughout the remainder of the study (Figure 1B). Concomitant with the increase in CCL5 expression, a time-dependent increase in $CD68^+$ macrophages and $CD3^+$ T lymphocytes in the interstitial space was observed (Figure 1A). Increased presence of macrophages and T lymphocytes was assessed quantitatively by RT-PCR (Figure 1C) and by western blot (Figure 1D). Expression of CD68 relative to β-actin increased from 0.19 to 1.31 at 1-week postinjury before dropping to 0.49 at 8 weeks postinjury. Expression of CD3 increased much more slowly, with a relative expression level of 0.63 at 4 weeks postinjury, rising to 2.24 by 8 weeks postinjury.

### Transplanted SRC attenuate NF-κB & PAI-1 activation & reduce macrophage & T-cell infiltration in the 5/6 nephrectomy model

Clinical outcomes associated with SRC treatment of 5/6$N_x$ rodents are summarized in Table 3. Statistically

significant improvement in glomerular function was observed at 12 weeks post-treatment, with serum creatinine dropping from 1.13 ± 0.15 to 0.70 ± 0.10 mg/dl. BUN dropped from 45.71 ± 5.41 to 36.33 ± 7.77 mg/dl. In addition, statistically significant improvement in tubular function was observed at 12 weeks post-treatment, with serum albumin levels rising from 2.84 ± 0.10 to 3.30 ± 0.10 g/dl. A:G ratio (albumin:globulin) rose from 0.80 ± 0.04 to 1.05 ± 0.12. No untreated animals survived the entire 6 month time-course. IHC analysis at time of death revealed intense, widespread expression and nuclear localization of p65 throughout

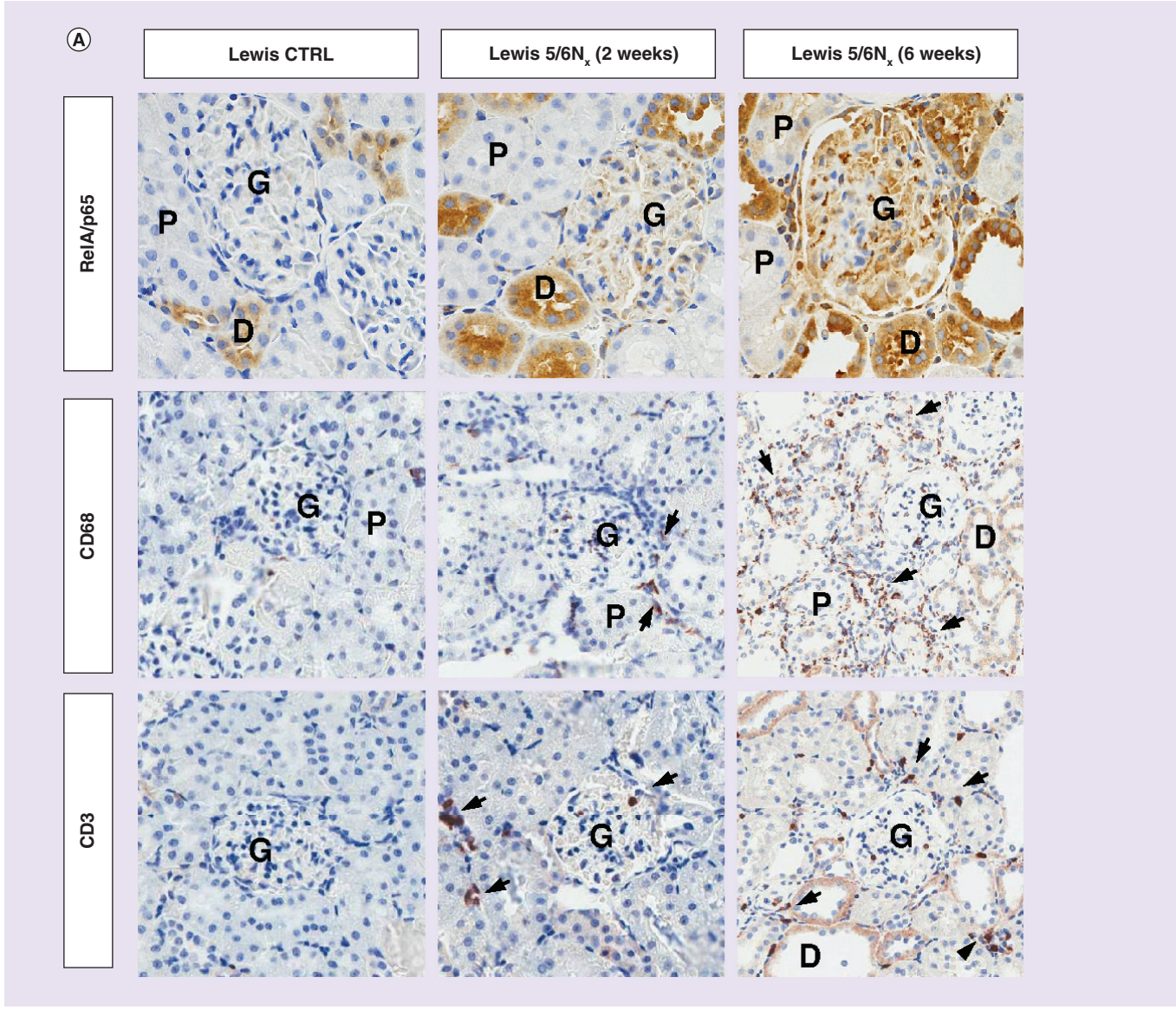


**Figure 1. Immunohistological and molecular characterization of 5/6 nephrectomy Lewis rat model.** Immunohistochemical staining for NF-κB subunit p65 in unmanipulated CTRL rats compared with animals subjected to 5/6 nephrectomy procedure (**[A]** top row). Nuclear staining (arrows) indicates NF-κB-activated cells. Infiltration of macrophages and T lymphocytes as identified by CD68 and CD3 immunostaining (arrows), respectively, is observed in nephrectomized animals at 2 and 6 weeks postprocedure (**[A]** middle and bottom rows). Whole tissue lysates were assayed for CCL5 by quantitative real-time PCR **(B)**. Increased presence of CD68 and CD3 expressing cells was confirmed by quantitative real-time PCR (**[C]**). Semiquantitative western blot analysis on whole kidney lysates at 1, 2, 4, 6 and 8 weeks postnephrectomy **(D)** demonstrates increased IκBα stability as well as increased presence of macrophages and T lymphocytes (CD68, CD3) with disease progression. Analysis of cytoplasmic ('C') and nuclear ('N') lysates from kidney tissues at 1, 2, 4, 6 and 8 weeks postnephrectomy **(E)** reveals progressive nuclear localization of the p65 subunit. LB1 is used as a nuclear fraction loading control. For western blots in **(D)**, band densities were quantified relative to internal control (β-actin) and are expressed below each band. For western blot in **(E)**, band densities were quantified by calculating the ratio N/C (nuclear p65/cytoplasmic p65). The N/C ratio for the control was set at 1 and all treatment conditions expressed relative to control.
CTRL: Control; D: Distal-convoluted tubule; G: glomerulus; $N_x$: Nephrectomy; P: Proximal-convoluted tubule.

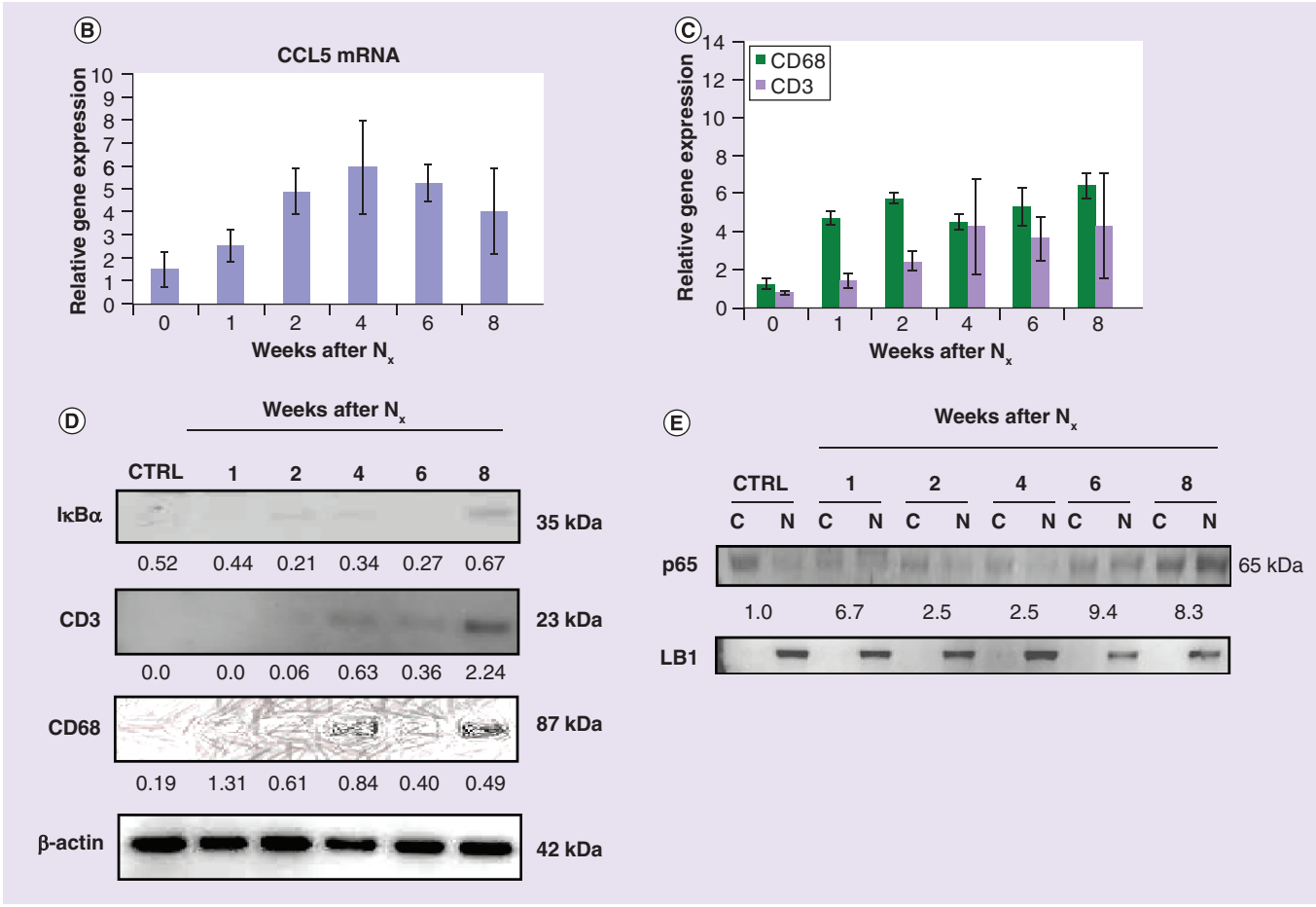


**Figure 1. Immunohistological and molecular characterization of 5/6 nephrectomy Lewis rat model (cont.).**

kidney tissue (Figure 2A). In addition, extensive infiltration of $CD68^+$ and $CD3^+$ leukocytes was observed (Figure 2A). Nuclear localization of p65 subunit was not widely observed in healthy, unilaterally nephrectomized animals and $CD68^+$ and $CD3^+$ cells were scarce in those tissues (Figure 2A). SRC-treated tissues displayed decreased p65 nuclear localization and reduced numbers of both $CD68^+$ and $CD3^+$ leukocytes, while B1/B5 (non-SRC cell control) treated animals resembled untreated disease state (Figure 2A). Quantitative IHC analysis at time of death of untreated animals in Lewis 5/6$N_x$ confirmed upregulation of NF-κB p65 and *PAI-1* expression. Treatment with SRC significantly reduced both NFkB-p65 and *PAI-1* expression levels (Figure 2B & C & Table 3). These observations were confirmed by gene-expression and western blot on whole lysates from representative tissue samples (Figure 2D & E). Quantitative western analysis of relative (to β-actin) *PAI-1* expression showed a significant reduction from 148.2 in nephrectomized animals at <100 days on study to 31.2 upon SRC treatment at <100 days on study. FN (another marker of fibrosis) levels were also reduced in SRC-treated animals (Figure 2E) at <100 days on study, with relative expression levels falling from 108 to 44 upon SRC treatment. Similar results were observed >100 days on study: relative *PAI-1* expression fell from 106.1 to 28.5 upon SRC treatment and relative FN expression levels dropped from 108.6 to 68.1.

Additional evidence demonstrating attenuation of NF-κB signaling in SRC-treated animals was provided by gene-expression and western blot analysis of nuclear localization of NF-κB p65. Compared with untreated 5/6$N_x$ controls and B1/B5-treated animals, SRC-treated tissues had reduced levels of nuclear p65 (Figure 2H). Quantitation of nuclear p65/cytoplasmic p65 was performed relative to hemi-$N_x$ control animals. As observed previously (Figure 1E), response to full 5/6$N_x$ is associated with significant cytoplasmic to nuclear transfer of p65, with relative expression levels increasing to 4.2 (Figure 2H) but reduced to 0.4 upon treatment with SRC. Treatment with B1/B5 only resulted in reduction to a relative expression level of 2.2. In addition, treatment with SRC reduced relative expression of CD3 from 0.70 (pre-treatment) to 0.22, comparable to the hemi-$N_x$ control expres-

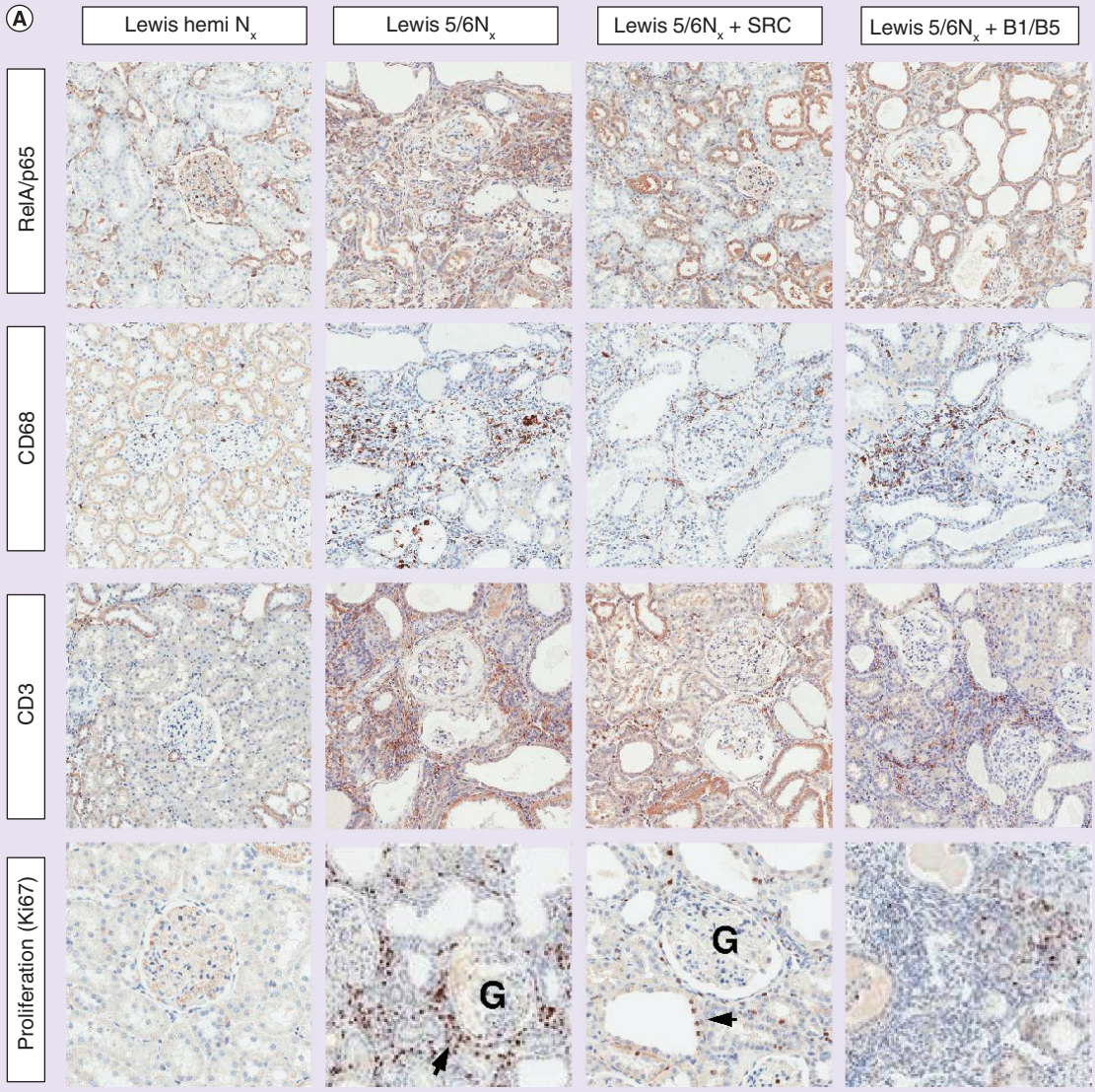


**Figure 2. Transplantation of selected renal cell into 5/6 nephrectomy model attenuates NF-κB activity and alters inflammatory profile of kidney.** Kidney tissue was harvested 6 month post-transplantation or at time of death, in rats treated with SRC or B1/B5 cells. Hemi-$N_x$ and 5/6$N_x$ animals were carried as healthy and diseased controls, respectively. Immunohistochemistry for the NF-κB p65 subunit, CD68, CD3 was performed to assess the inflammatory state of tissues **[A]**, top three rows). Cellular proliferation in tissues was determined by Ki67 immunostaining **[A]**, bottom row). Tissue protein levels of NF-κB p65 subunit and PAI-1 at end-of-study were significantly reduced in 5/6$N_x$ + SRC animals **[B]**, magnification 20× and 200× in-lay) compared with untreated controls by quantitative immunohistochemistry **[C]**, quantitation of PAI-1 and NF-κB p65 staining, n = 3). Tissue lysates (n = 3, except n = 2 for B1/B5 treatment) were assayed for *CCL5* expression by quantitative real time-PCR **(F)** and *CCL2* expression by ELISA **(G)**. Error bars represent standard error of mean in each experimental group. Quantitative real time-PCR was conducted on kidney tissue harvested at necropsy and relative gene-expression values plotted against time (days) on study. 5/6$N_x$ animals (red squares) demonstrated more robust expression of PAI-1 relative to those treated with bioactive renal cells (blue diamonds) and sham-operated controls (green triangles) **(D)**. Representative western blot analysis of kidney samples taken at 3 and 6 months post-treatment. Treated tissues of 5/6$N_x$ rats ($N_x$ + SRC) showed reduced accumulation of PAI-1 and FN protein, normalized to β-actin by the formula: (intensity PAI1 or FN/intensity β-actin) ×100 **(E)**. Western blot analysis confirmed increased nuclear localization of NF-κB p65 **(H)** in diseased and B1/B5-treated rats compared with healthy and SRC-treated rats. Reduction of nuclear p65 corresponded with decreased IκBα, CD3 and CD68 **(I)**. For western blot in 1H, band densities were quantified by calculating the ratio N/C (nuclear p65/cytoplasmic p65). The N/C ratio for the control (hemi-Nx) was set at 1 and all treatment conditions expressed relative to control. In **(I)**, quantitation of band density shown as (intensity marker/intensity β-actin).
C: Cytoplasm; Hemi: Unilateral; N: Nucleus; $N_X$: Nephrectomy; Sham: Sham surgery; SRC: Selected renal cell.

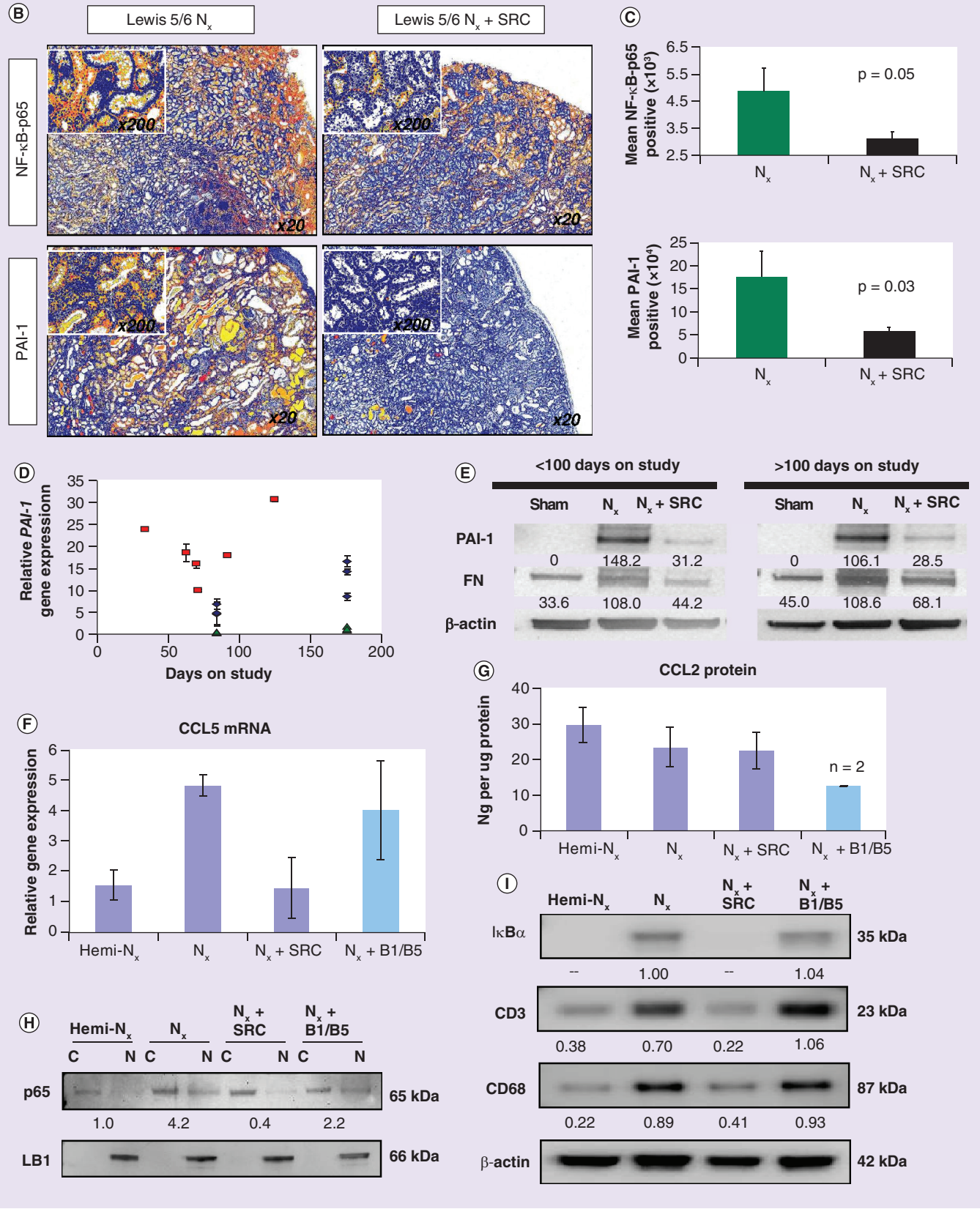


**Figure 2. Transplantation of selected renal cell into 5/6 nephrectomy model attenuates NF-κB activity and alters inflammatory profile of kidney (cont.).**

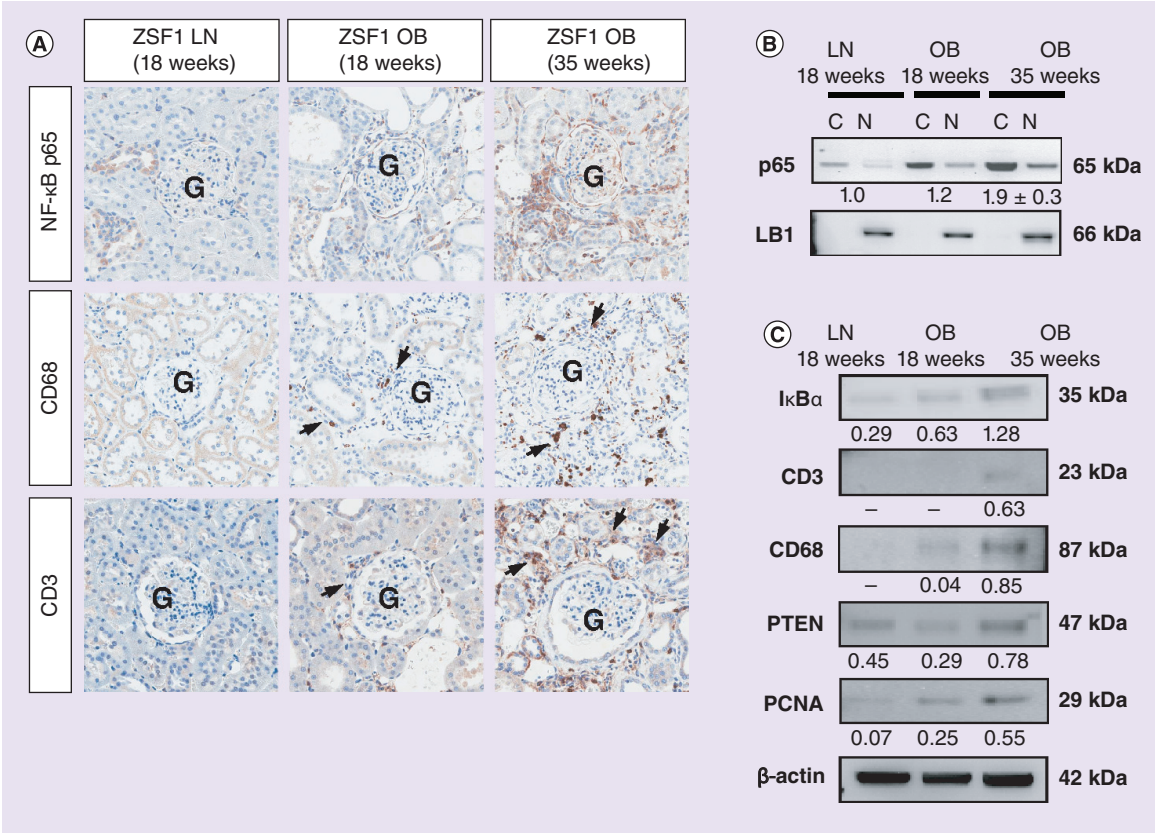


**Figure 3. Immunohistochemical and molecular characterization of ZSF1 rat model.** Kidney tissues from lean, 18-week-old ZSF1 rats were compared with obese ZSF1 rats at 18 and 35 weeks of age. Immunostaining for p65, CD68 and CD3 demonstrate increased inflammatory states in diseased animals, which increases over time (**[A]**, arrows). Western blot analysis for nuclear p65 **(B)**, as well CD68 and CD3 in whole lysates, confirms those observations **(C)**. IκBα, PTEN and PCNA also increase in diseased tissues and are dependent on age **(C)**. For western blot in **(B)**, band densities were quantified by calculating the ratio N/C (nuclear p65/cytoplasmic p65). The N/C ratio for the control (LN, 18 weeks) was set at 1 and all treatment conditions expressed relative to control. In **(C)**, quantitation of band density shown as (intensity marker/intensity β-actin).
C: Cytoplasm; G: Glomerulus; LN: Lean; N: Nucleus; OB: Obese.

sion level of 0.38. By contrast, treatment with B1/B5 resulted in an increase of CD3 relative expression levels to 1.06 (Figure 2I). Similarly, SRC treatment reduced expression of CD68 from 0.89 to 0.41 (relative to β-actin), comparable to the hemi-$N_x$ control expression level of 0.22, whereas treatment with B1/B5 caused an increase in CD68 relative expression to 0.93 (Figure 2I). Finally, CCL5 gene-expression levels in SRC-treated rats were comparable to untreated healthy controls (Figure 2F), while CCL2 expression remained unaltered (Figure 2G).

## Transplanted SRC promote tubular cell proliferation in 5/6$N_x$ rats

Rodent tissues were evaluated by immunohistochemistry for the cell cycle marker Ki67. SRC treatment increased the number of proliferating cells specifically in the tubular epithelia (Figure 2A). By comparison, few $Ki67^+$ epithelial cells were observed in untreated and B1/B5-treated kidneys. However, several proliferative cells were observed in the interstitial compartment (Figure 2A), see also Table 3.

## Transplanted SRC attenuate NF-κB signaling & PAI-1 expression in ZSF1 model of DN

Clinical outcomes associated with SRC treatment of ZSF1 rodents are summarized in Table 4. Statistically, significant improvement in glomerular function was observed at 16 weeks post-treatment, with serum creatinine dropping from 53 ± 2.7 to 44.2 ± 1.8 μmol/l. BUN dropped from 11.42 ± 0.75 to 8.21 ± 0.61 mmol/l. In addition, statistically significant improvement in tubular function was observed at 24 weeks post-treatment, with excreted calcium levels dropping from 3.02 ± 0.04 to 2.87 ± 0.03 mmol/l. Excreted phosphorus dropped from 2.23 ± 0.08 to 1.97 ± 0.06 mmol/l. Finally, biomarkers associated with function of the Loop of Henle and collecting ducts

also showed statistically significant improvement at 16 weeks post-treatment, with urine osmolality increasing from 681 ± 48.7 to 901 ± 41.6 mOsmol/kg and urine specific gravity increasing from 1.034 ± 0.001 to 1.040 ± 0.001. Baseline indices for all renal biomarkers in the ZSF1 model are reported in [23].

To ascertain the involvement of NF-κB signaling in progression of CKD in a different rodent model, we conducted molecular analysis on tissues derived from ZSF1 lean (i.e., nondiseased) and obese (i.e., diseased) rats. IHC analysis of kidneys revealed that by 18 weeks of age, obese rat kidney tissues are more highly activated for NF-κB pathways compared with lean littermates based on the increased expression and nuclear localization of the p65 subunit (Figure 3A). By 35 weeks of age, obese rats demonstrated more robust NF-κB activation compared with 18-week-old obese rats, reflecting the progressive nature of DN (Figure 3A). Western blot analysis was performed on cytoplasmic and nuclear extracts from 18-week-old lean, 18-week-old obese and 35-week-old obese rat kidneys to semiquantitatively assess the activation levels of NF-κB. Transfer of p65 from cytoplasm to nucleus was observed during development of the diabetic condition in the ZSF1 rodent: By 35 weeks, the ratio p65(nucleus)/p65(cytoplasm) in the obese animal had increased to 1.9 relative to the lean rodent at 18 weeks (Figure 3B). This was accompanied by increases in the relative expression levels of IκBα (increased from 0.29 in lean rodents at 18 weeks to 1.28 in obese rodents at 35 weeks), CD3 (increased from 0 in lean rodents at 18 weeks to 0.63 in obese rodents at 35 weeks), CD68 (increased from 0 in lean rodents at 18 weeks to 0.85 in obese rodents at 35 weeks), PTEN (increased from 0.45 in lean rodents at 18 weeks to 0.78 in obese rodents at 35 weeks) and PCNA (increased from 0.07 in lean rodents at 18 weeks to 0.55 in obese rodents at 35 weeks) (Figure 3C). This analysis confirmed that expression and nuclear localization of p65 as well as other proinflammatory markers including IαBα increased in obese rats over time.

IHC analysis on 18-week-old lean, 18-week-old obese and 35-week-old obese rat kidneys for expression of CD68 and CD3 showed an increased presence of monocytes/macrophages and T lymphocytes in the peritubular and periglomerular spaces in obese kidney tissues compared with lean control tissues (Figure 3A). The number of leukocytes increased over time in diseased animals. Tissue levels of PAI-1 were measured at end stage of disease using quantitative IHC analysis of ZSF1 obese untreated and SRC-treated animals. As observed in 5/6N$_x$ rats, SRC treatment was associated with reduction in expression of urinary CCL5 (but not urinary CCL2), NF-κBp65 and PAI-1 (Figures 4A & B & 5A & B).

## CM from human SRC can attenuate NF-κB activation *in vitro* independent of vesicle-mediated cell signaling

To mimic the disease state, HK2 cells were cultured for 30 min with TNF-α to drive NF-κB activation. We tested NF-κB activation by exposing HK2 cells to 10 ng/ml TNF-α under serum- and supplement-free conditions and assayed for nuclear localization of p65 by immunofluorescence (Figures 6A & B & 7A).

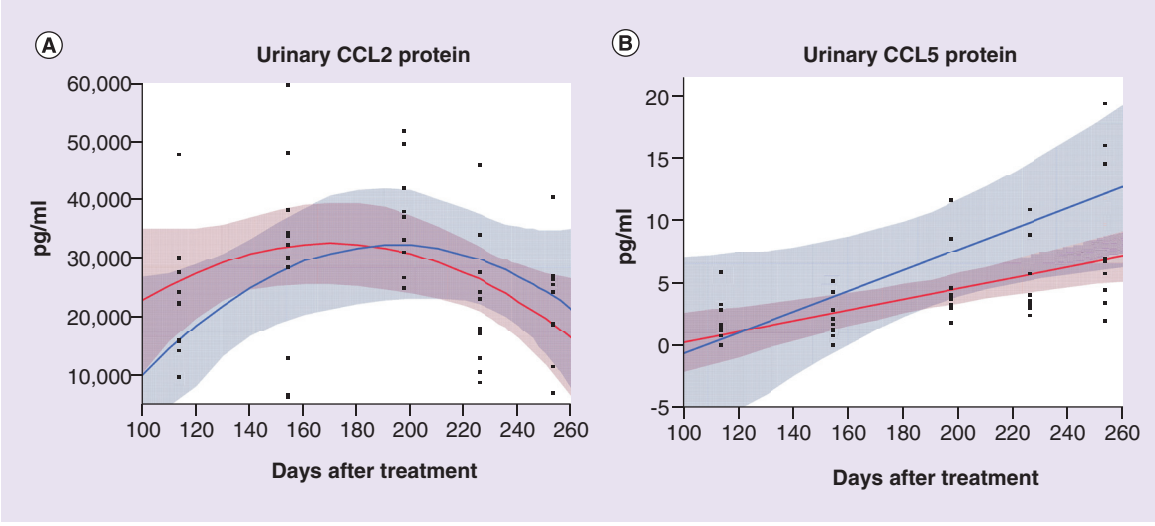


**Figure 4. Urinary cytokines in ZSF1 rats treated with selected renal cell.** Urinary **(A)** CCL2 and **(B)** CCL5 as a measure of tissue-level inflammatory states of the kidney were assayed by ELISA at regular intervals over the course of the study. Based on these data, multivariable models were generated by JMP version 7.0 software, with the blue-shaded regions representing modeled cytokine excretion (CCL2, CCL5) in untreated ZSF1 obese rats (n = 5) and the red-shaded region representing modeled cytokine excretion in selected renal cell-treated ZSF1 obese rats (n = 7).

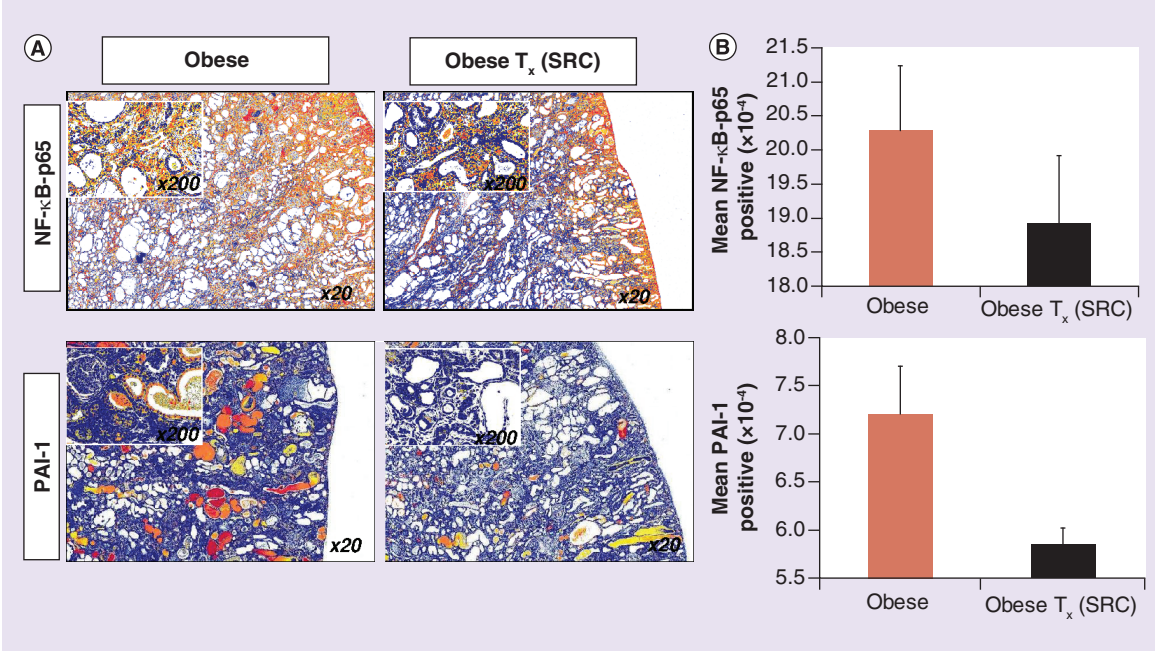


**Figure 5. Immunohistochemical analysis of ZSF1 rats treated with selected renal cell.** Tissue protein levels at end of study of NF-κB-p65 subunit and PAI-1 were significantly reduced in ZSF1-obese-treated animals (**[A]**, magnification 20× and 200× in-lay) compared with untreated controls by quantitative immunohistochemistry (**[B]**, n = 3).
SRC: Selected renal cell; $T_x$: Treatment.

Preincubating HK2 cells with CM derived from unfractionated renal primary cells for 2 h was effective in attenuating TNF-α-induced p65 nuclear localization response (Figure 7A). Nuclear-localized p65 in HK2 cells (sum of low and high activation) under basal control conditions was observed in approximately 30% of culture and increased to approximately 50% upon TNF-α stimulation. SRC-CM reduced p65 nuclear localization (sum of low and high activation) in unstimulated cells to approximately 12%, but did not alter percentage of total p65 nuclear localization after addition of TNF-α (activation remaining at approximately 50%). However, SRC-CM reduced total percentage of highly activated cells from 32% (basal media with TNF-α) to 16% (SRC-CM + TNF-α) (Figure 7B). Western blot analysis confirms primary renal cell-derived CM attenuated TNF-α-mediated NF-κB activation, shown by reduced presence of both p65 and p50 subunits in nuclear lysates (Figure 7C).

*In vitro* experiments were repeated using an HK2 line containing NF-κB reporter construct with luciferase gene-expression under control of five tandem repeats of NF-κB response elements (Promega). Here, TNF-α induced robust dose-dependent luciferase expression after 4 h of incubation (Figure 8A). Cells preincubated with SRC-CM for 24 h prior to activation showed significant reduction in basal luciferase activity (Figure 8A) and this suppressive activity was maintained at TNF-α exposures of 0.1, 1.0 and 10 ng/ml. To identify bioactive component(s) of SRC-CM responsible for NF-κB attenuation capacity, media was subjected to ultracentrifugation at 200,000 g. Supernatant media was depleted of large particles (including secreted vesicles) while still containing soluble proteins and metabolites. This VFM was sufficient to reduce NF-κB activation *in vitro* at a magnitude comparable to noncentrifuged SRC-CM (Figure 8A). Components of the 200,000 g pellet were resuspended in serum- and supplement-free media, concentrating the components by a factor of five. This pellet was unable to attenuate NF-κB activity (Figure 8A). These data indicate that NF-κB suppressor(s) contained within SRC-CM are not directly associated with secreted vesicles.

In order to further identify bioactive component(s), vesicle-free CM was fractionated by passing samples through semipermeable polyethersulfone membranes with MWCO at 5–100 kDa. This strategy was employed to narrow down sizes of bioactive particle(s) present in CM. Each flow-through fraction was tested for capacity to inhibit NF-κB reporter activity *in vitro*. 100 and 50 kDa filtrates retained suppressive activity on TNF-α-induced NF-κB (data not shown). However, 10 and 5 kDa membranes did not eliminate NF-κB-suppressive

component (Figure 8B), indicating that the bioactive component is smaller than 5 kDa.

### Secreted vesicles in CM from rat & human SRC can attenuate PAI-1 expression *in vitro*

CM from rat and human SRC attenuated expression of PAI-1 from cultured HRMC induced (+) and uninduced (-) with TGF-β1 (Figure 9A & B). To identify bioactive component(s) of SRC-CM responsible for PAI-1 attenuation capacity, media was subjected to ultracentrifugation at 200,000 g. CM supernatant collected postcentrifugation was less effective at attenuating PAI-1 expression relative to control CM (Figure 9A & B), suggesting that the CM component responsible for observed attenuation of PAI-1 protein is associated with an insoluble cellular element.

To evaluate this hypothesis, we have examined the miRNA profile of secreted vesicles isolated from human and rodent SRC-CM against PCR arrays of established miRNAs. A detailed characterization of the SRC-CM miRNA profile will be published elsewhere [Basu *et al.* (2016), Manuscript in Preparation]. In the current manuscript, we analyze miRNAs specifically and directly linked to the PAI-1/NF-κB signaling pathway.

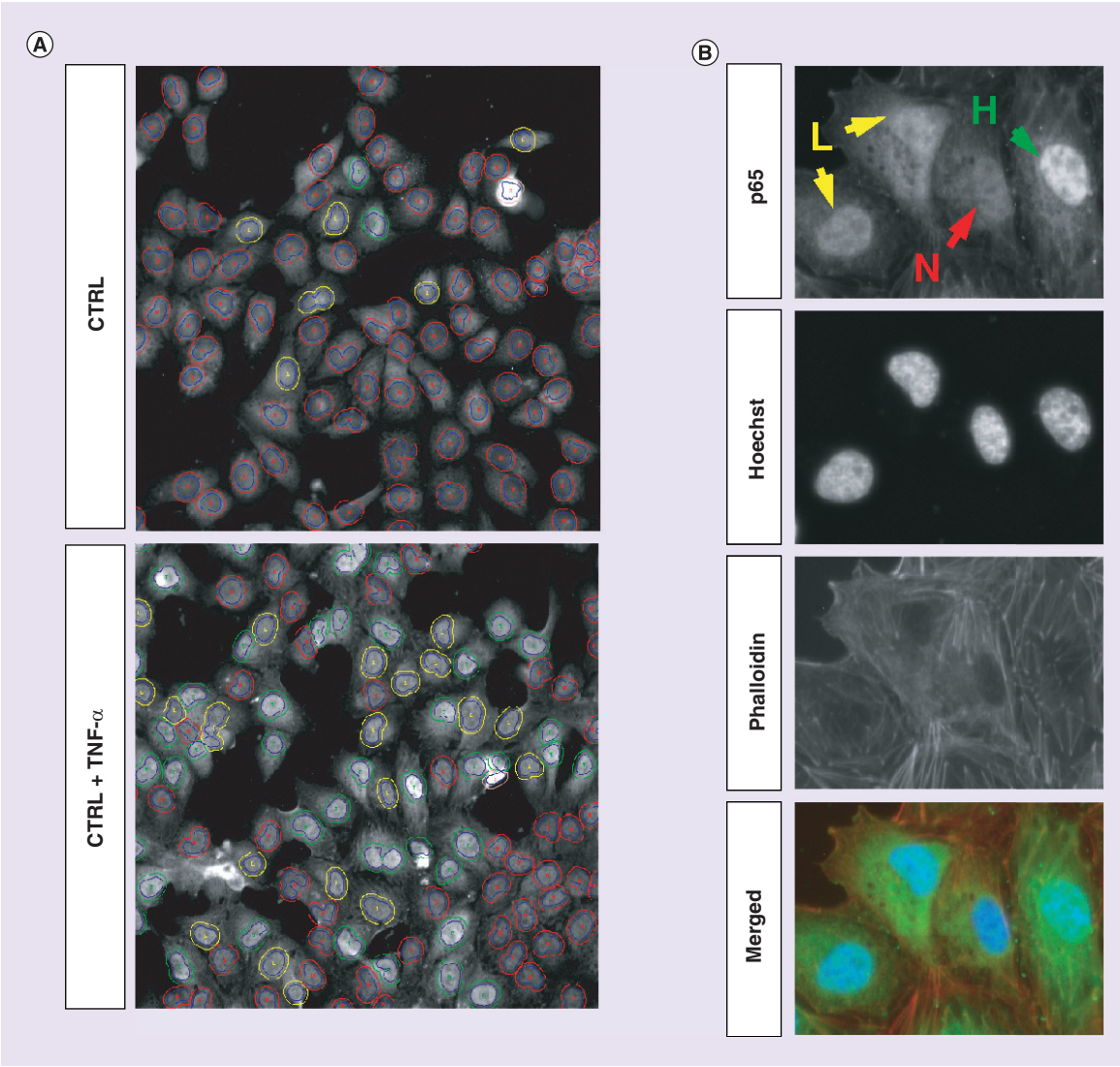


**Figure 6. Quantification of p65 nuclear localization. (A)** Cells that were untreated or treated with 10 ng/ml TNF-α were assessed for NF-κB activation by p65 immunofluorescence. Grayscale images were taken at 200× magnification, and analyzed with a classifier filter based on nuclear intensity. Nuclear boundaries (blue lines) were defined by Hoescht dye. Red lines identify 'N', yellow lines identify 'L' and green lines identify 'H'. **(B)** Higher power view of representative cells that were categorized as 'N' (red), 'L' (yellow) and 'H' (green). Cells were counterstained with Hoescht dye to define nuclear boundaries and Alexa-Fluor 594-phallodin to better visualize individual cells **(B)**.
CTRL: Control; H: High activation; L: Low activation; N: No activation.

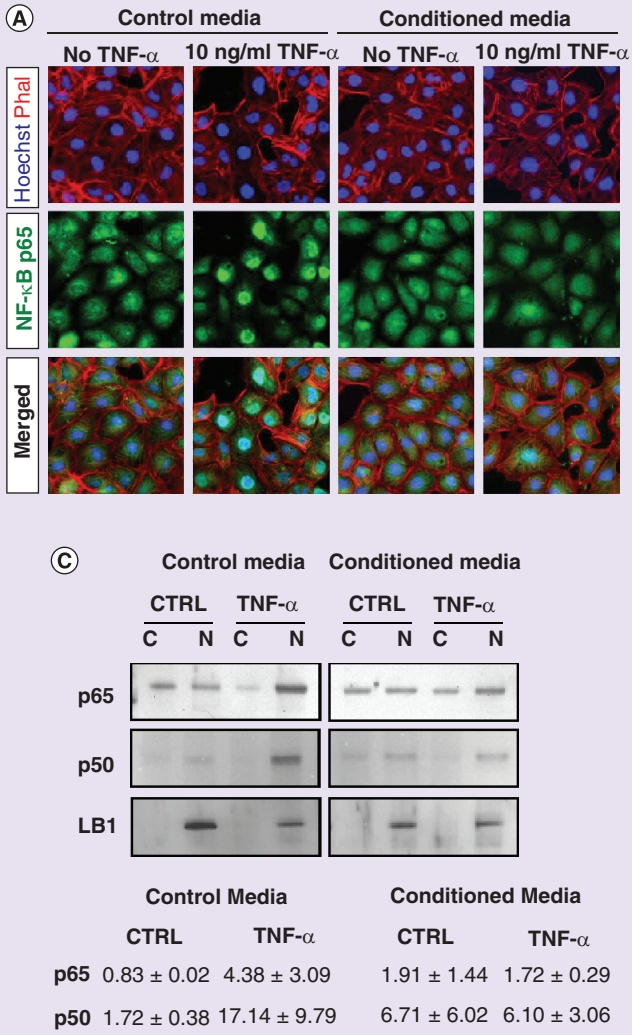


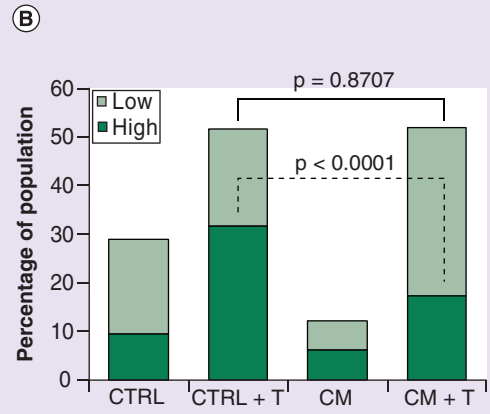


| | No activation (<110 units) | | Low activation (110–130 units) | | High activation (>130 units) | |
|---|---|---|---|---|---|---|
| **CTRL** | 213/299 | 71.2% | 59/299 | 19.7% | 27/299 | 9.0% |
| **CTRL TNF-α** | 174/362 | 48.1% | 72/362 | 19.9% | 116/362 | 32.0% |
| **CM** | 258/293 | 88.1% | 18/293 | 6.1% | 17/293 | 5.8% |
| **CM TNF-α** | 135/274 | 49.3% | 94/274 | 34.3% | 45/274 | 16.4% |

**Figure 7. Extracellular factors attenuate NF-κB activation in target epithelial cells. (A)** Immunofluorescence assay to determine nuclear localization of p65 (Alexa-Fluor 488, green) in HK2 cells that were unstimulated or stimulated with 10 ng/ml TNF-α for 30 min. Cells were counterstained with Hoechst (blue) and Alexa-Fluor 594-phalloidin (red). Cells were pretreated with basal media or CM from selected renal cell for 2 h prior to TNF-α induction. **(B)** All cells from three fields of view for each condition were classified into three categories (high activation, low activation and no activation) based on staining intensity for p65 and plotted as percentages of the total cell populations. **(C)** Western blot analysis confirms that pretreating HK2 cells with selected renal cell-CM can reduce nuclear localization of p65 as well as NF-κB-p50 subunit. LaminB1 was used as a nuclear fraction ('N') loading CTRL and was not detected in cytoplasmic extracts ('C'). Quantitation of the blot is through the formula intensity (p65/p50 N)/intensity (p65/p50 C).
C: Cytoplasm; CM: Conditioned media; CTRL: Control; N: Nucleus; T: TNF-α.

miR-449a, a possible regulator of PAI-1 [33,34], was identified for additional functional evaluation. Other miRNAs of interest include miR-21 (RNA target: Pellino-1), miR-146a (RNA target: IRAK/TRAF6), miR-30b-5p (both regulators of PAI-1), miR-124 and miR-151 (RNA target: NF-κB). To evaluate the potential functional role of miR-449a, HRMC were transfected with miR-449a and exposed to 5 ng/ml TGF-β1 for 24 h. The expression of PAI-1 and β-actin by was evaluated by western blot. As shown in Figure 9C, transfection of synthetic miR-449a reduced TGF-β-induced expression of PAI-1 protein (from a relative expression level of 1.68 to 1.09, Figure 9C).

## Nonvesicle components of SRC-CM induce tubular cell proliferation

Near-confluent monolayers of HK2 cells were cultured with SRC-CM or basal control media for 24 and 48 h and assayed by qRT-PCR for cell cycle genes Cyclin D1, and *FOS*. SRC-CM increased Cyclin D1 gene-expression approximately twofold after 48 h of culture compared with basal media con-

trols (Figure 10A). *FOS* gene-expression was increased approximately twofold at 24 h, but returned to a level comparable to control media after 48 h of culture (Figure 10B). To determine if trophic factors were vesicle-associated components, we depleted SRC-CM by ultracentrifugation at 200,000 g. As before, pelleted vesicles were resuspended in basal media and concentrated fivefold. Direct comparison between vesicle-rich and vesicle-depleted SRC media shows proliferation (assessed by Cyclin D1 and *FOS*) is enhanced in target epithelia by nonvesicular factors (Figure 10A & B).

## Discussion

We have previously established the therapeutic effects of autologous native renal cells isolated from kidney tissue as primary cultures in progressive models of CKD; a summary of the overall study design is presented in Tables 1 & 2, and specific clinical outcomes in these rodent models are described in detail in [21–23,29], and will not be repeated here. However, specific mechanistic pathways and networks leading to observed disease-related outcomes within these models remain undefined, with concomitant ambiguity regarding MOA of SRC-based therapies under evaluation. Two-step 5/6 nephrectomy (5/6N$_x$) in rodents reproducibly generates terminally progressive renal failure with characteristic systemic and histological parameters of CKD (e.g., hypertension, reduced glomerular filtration rate, elevated serum creatinine and BUN, glomerular and tubulointerstitial fibrosis, hyperlipidemia, hyperphosphatemia and anemia) [21–23]. These clinically relevant features of the 5/6N$_x$ model combined with technical reproducibility and commercial availability provide the basis for its selection as a disease model for CKD. In addition, diabetes is the most important risk factor for CKD and ESRD. We have previously evaluated function, structure and lifespan of the ZSF1 diabetic rodents and demonstrated clinically relevant functional outcomes from SRC-cell therapy [23]. Extension in ZSF1 rodent survival following SRC treatment was accompanied by significant improvements to renal structure and function in multiple renal tissue niches [23].

Direct injection of these bioactive renal cell subpopulations in the rat 5/6N$_x$ model of CKD resulted in extended survival and enhancement of renal function for 6 month post-treatment [22]. That study also presented evidence that a potential MOA by which regenerative outcomes in the treated tissue occurred was consistent with mechanistic models currently under consideration for the therapeutic action of adult-derived stem cells [16,35–36]. Such MOAs leverage paracrine factors secreted by bioactive adult-derived cells to catalyze the mobilization of resident, host-derived stem cell populations, to ameliorate fibrosis and inflammation, to facilitate angiogenesis and neo-vascularization,

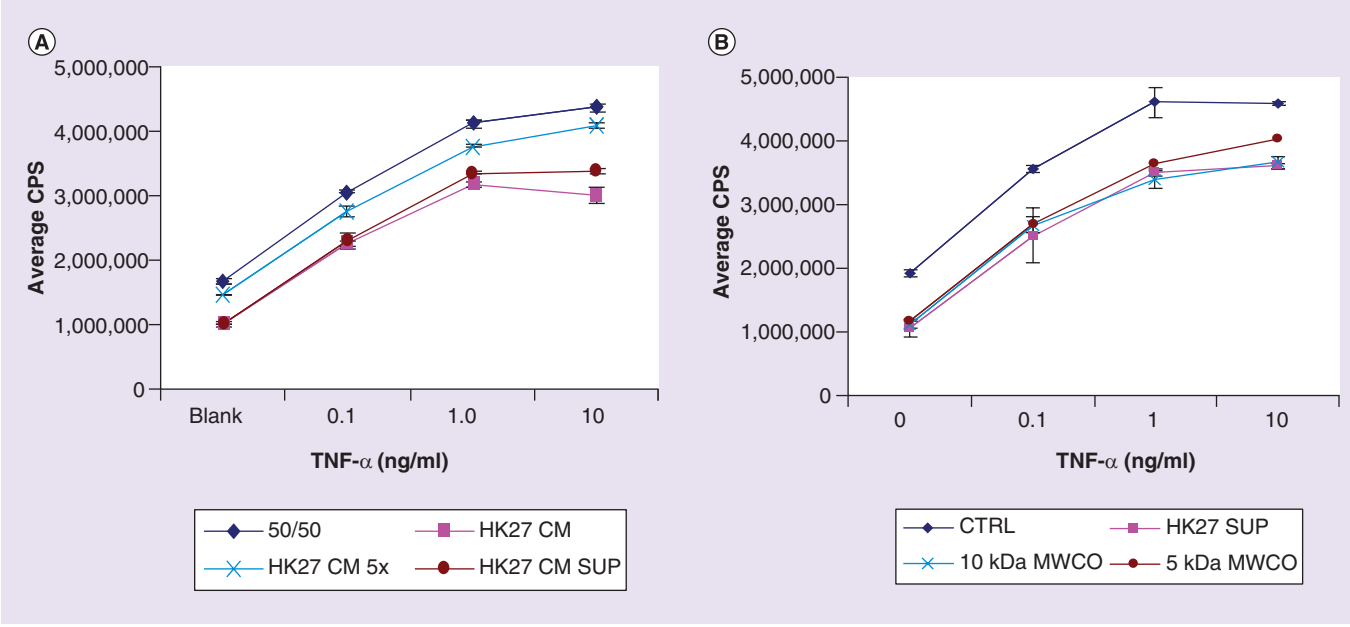


**Figure 8. Nonvesicle components of selected renal cell-conditioned media inhibit TNF-α-mediated NF-κB activation. (A)** HK2 cells transfected with an NF-κB luciferase reporter construct were pretreated for 16 h with basal media or CM from selected renal cell then subsequently stimulated with TNF-α for 4 h. The NF-κB inhibitory component is associated with the nonvesicular components of the CM. **(B)** Size exclusion based on MWCO of 10 and 5 kDa revealed that the NF-κB inhibitory component is smaller than 5 kDa. Error bars represent the standard deviation of three experimental replicates.
CM: Conditioned media; CPS: Counts per second; CTRL: Control; MWCO: Molecular weight cutoffs; SUP: Supernatant.

and to modulate the immune response. Evidence for the mobilization of resident stem cell populations in rodent 5/6$N_x$ CKD models following SRC treatment has been provided by studies showing activation of key markers associated with host stem cell populations upon SRC implant [29]. Engraftment of delivered SRC has been established up to 6 months postimplantation only in the targeted kidney [21–23]. Consistent with paracrine-based models of MSC bioactivity and experimental evidence that SRC produce factors that can potentially alter the balance between fibrosis and regenerative pathways in diseased kidney tissue are the secretomic profiles of bioactive renal cell populations [37]. Both SRC in 2D culture and 3D culture

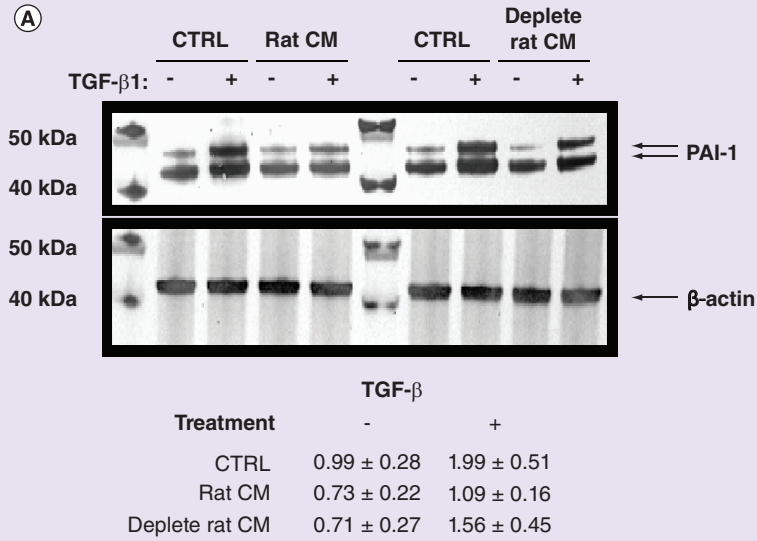


| Treatment | - | + |
|---|---|---|
| CTRL | 0.99 ± 0.28 | 1.99 ± 0.51 |
| Rat CM | 0.73 ± 0.22 | 1.09 ± 0.16 |
| Deplete rat CM | 0.71 ± 0.27 | 1.56 ± 0.45 |

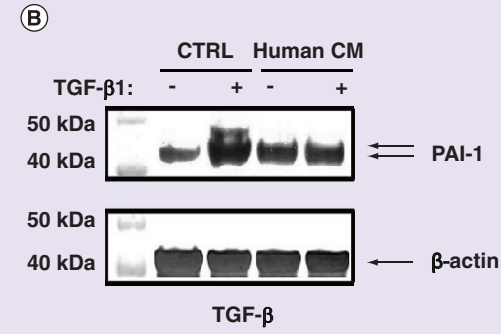


| Treatment | - | + |
|---|---|---|
| Control media | 0.89 ± 0.15 | 1.84 ± 0.13 |
| Human conditioned | 0.71 ± 0.15 | 1.35 ± 0.13 |

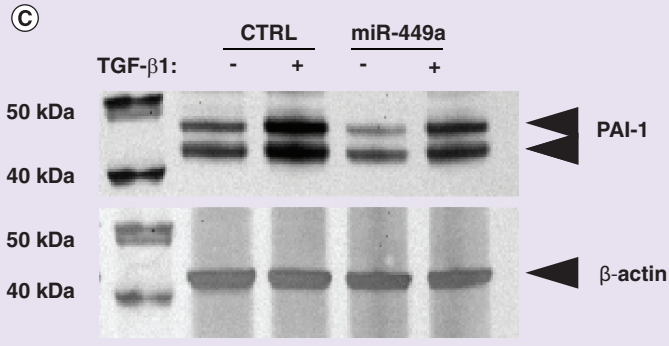


| Treatment | - | + |
|---|---|---|
| CTRL | 0.46 ± 0.23 | 1.68 ± 0.26 |
| miR-449a | 0.50 ± 0.30 | 1.09 ± 0.07 |

**Figure 9. Vesicle components of selected renal cell-conditioned media attenuate PAI-1 induced by TGF-β1 signaling.** *In vitro* experiments were designed to mimic the treatment effect of selected renal cell (SRC) observed *in vivo*. Human-derived renal mesangial cells (HRMC) control express increased levels of PAI-1 in the presence (+) of 5 ng/ml TGF-β1. **(A)** CM from rat SRC modulates PAI-1 expression in cultured HRMC induced (+) and uninduced (-) with TGF-β1. **(B)** HRMC cocultured with CM derived from human SRC attenuates TGF-β1-induced PAI-1 protein expression. Secreted vesicles from human and rat SRC-CM were collected by high-speed centrifugation and assayed for miRNA content using PCR-based arrays of known sequences. miR-449a, a putative regulator of PAI-1 was identified. HRMC were transiently transfected with miR-449a or not (CTRL). **(C)** 24-h post-transfection HRMC were either exposed to 5 ng/ml TGF-β1 (+) or not (-) for an additional 24 h. Total protein was prepared and assayed for PAI-1 and β-actin by western blot. miR-449a reduced basal and induced PAI-1 protein expression. For **(A–C)**, quantitation of band density shown as (intensity PAI-1/intensity β-actin).
CM: Conditioned media; CTRL: Control.

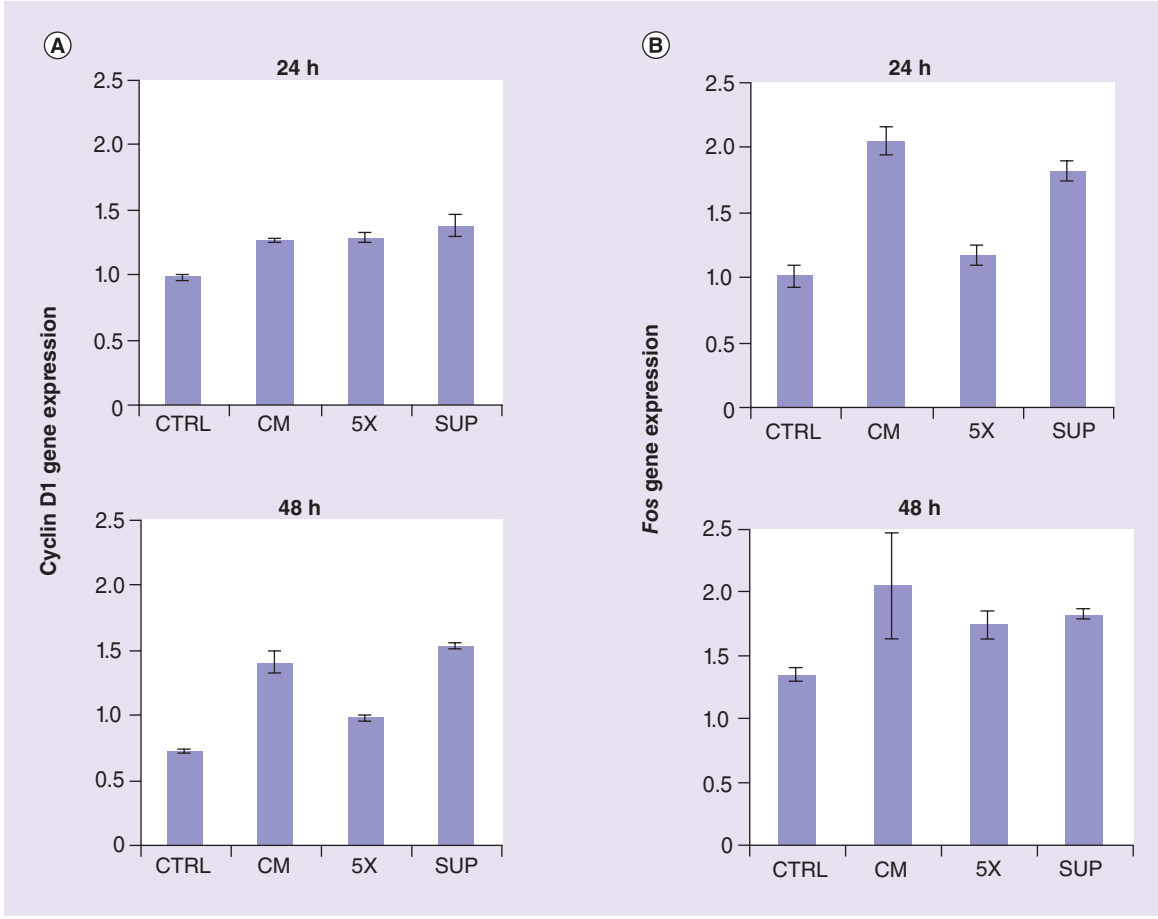


**Figure 10. Selected renal cell-conditioned media promotes proliferation independently from secreted vesicles.**
HK2 cells were cultured in selected renal cell (SRC)-CM for 24 and 48 h, and assayed by quantitative real-time PCR for cell cycle markers Cyclin D1 **(A)**, *FOS* **(B)**. Basal media was used as a negative CTRL. Vesicle-associated components of the media were separated from SRC-CM and concentrated by ultracentrifugation by a factor of 5 (5X). Vesicle-deplete CM was collected from the SUP. Error bars represent the standard error of the mean of three experimental replicates.
CM: Conditioned media; CTRL: Control; SUP: Supernatant.

express genes and/or proteins of numerous therapeutically relevant cytokines and growth factors, including PDGF-ββ, VEGF, NGF, GDNF, the matrix metalloproteinases MMP-1, MMP-9, TIMP-1 and MCP-1, which have been shown to mediate such paracrine effects [37].

Here, we have characterized progressive NF-κB activation and interstitial inflammation during development of etiology in the 5/6$N_x$ model from 1 to 8 weeks postsurgery. A time-dependent increase in expression and nuclear localization of NF-κB p65 was observed, particularly during chronic phases of disease progression (2–8 weeks postnephrectomy). At 6 weeks postnephrectomy, robust p65 nuclear localization was observed in tubular epithelial and glomerular cells indicating that those particular cellular compartments were subjected to cellular stressors (Figure 1A). SRC product potency prior to cell transplantation was evaluated by functional characterization of B2-associated megalin:cubilin-mediated albumin transport and GGT1 activity. These bioassays demonstrated that the expression of cubilin and GGT1 was associated with functionally active protein. Interference by RAP, an established competitive inhibitor of megalin:cubilin-mediated albumin transport and the observed lack of albumin uptake in nontubular B4 subpopulation [22] confirmed the specificity of albumin transport. Observed functional outcomes met previously established pass/fail criteria for SRC product release [38, 39] and SRC was therefore found acceptable for cell transplantation.

Transplanted SRC was observed to attenuate NF-κB activation and reduce macrophage and T-cell infiltration. As shown in Figure 2A, SRC-treated tissues displayed decreased p65 nuclear localization and reduced numbers of both $CD68^+$ and $CD3^+$ leukocytes, while B1/B5 (non-SRC cell control) treated animals resembled untreated disease state. Additionally, trans-

Table 5. Quantitative histological analysis of impact of selected renal cell and B1/B5 treatment of 5/6 nephrectomized rodents.

| | Group | NF-κB-p65 | CD3 | CD68 | Ki-67 |
|---|---|---|---|---|---|
| **Rat ID#** | | | | | |
| 199 | 1 | 1 | 1 | 0 | 0 |
| 200 | 1 | 1 | 1 | 1 | 0 |
| 201 | 1 | 1 | 1 | 1 | 0 |
| 183 | 2 | 3 | 4 | 4 | 2 |
| 188 | 2 | 2 | 4 | 3 | 2 |
| 193 | 2 | 3 | 4 | 4 | 4 |
| 169 | 3 | 2 | 2 | 2 | 3 |
| 174 | 3 | 2 | 2 | 2 | 3 |
| 159 | 3 | 3 | 3 | 3 | 1 |
| 171 | 3 | 3 | 4 | 3 | 2 |
| 181 | 3 | 1 | 2 | 2 | 3 |
| 168 | 4 | 3 | 3 | 2 | 2 |
| 182 | 4 | 3 | 3 | 3 | 2 |
| 195 | 4 | 2 | 4 | 2 | 3 |
| **Rat treatment** | | | | | |
| Hemi-NX | 1 | (n = 3) | | | |
| $5/6N_x$ | 2 | (n = 3) | | | |
| $5/6N_x$ + SRC | 3 | (n = 5) | | | |
| 5/6 + B1/B5 | 4 | (n = 3) | | | |

Grade 0 (absent/normal): This score reflects a focal, multifocal or diffuse distribution in which approximately 0–5 cells are staining positive per high power field (HPF; 40×).
Grade 1 (minimal): This score reflects a focal, multifocal or diffuse distribution in which approximately 5–10 cells are staining positive per HPF (40×).
Grade 2 (mild): This score reflects a focal, multifocal or diffuse distribution in which approximately >10–25 cells are staining positive per HPF (40×).
Grade 3 (moderate): This score reflects a focal, multifocal or diffuse distribution in which approximately >25–40 cells are staining positive per HPF (40×).
Grade 4 (marked): This score reflects a focal, multifocal or diffuse distribution in which approximately >40 cells are staining positive per HPF (40×).

planted SRC promotes tubular cell proliferation in the $5/6N_x$ model. SRC treatment specifically increased the number of $Ki67^+$ proliferating cells specifically in the tubular epithelia (Figure 2A & Table 5). This compartment-specific proliferation may be a direct indicator of therapeutic outcome: epithelial proliferation leads to replenishment of renal function, while interstitial proliferation leads to fibrosis. Given that proliferation occurs in a compartment-specific manner (Figure 2A & Table 5), increase in proliferation in SRC-treated kidneys is primarily in renal epithelium and not interstitium. Consistent with models described in [40,41], the simplest explanation of these data is that these proliferative cells are endogenous tubular epithelial cells that have been stimulated by SRC to divide and migrate to the sites of cellular injury and fibrosis.

Multiple established biomarkers of renal inflammation and injury may potentially be interrogated to evaluate the disease condition. As discussed in [38,39], expression of the kidney injury marker KIM1 is currently being leveraged as a potency marker and release criterion metric for SRC in ongoing Phase I clinical trials. Secretomic profiling of SRC has identified additional biomarkers potentially relevant for monitoring progress of renal disease. These include: α1MG, β2MG, calbindin, clusterin, CTGF, Cystatin C, GST-α, NGAL, osteopontin, TFF3, TIMP-1, VEGF, ANG2, PDGF-ββ, ICAM, MCP-1, MMP-9, PAI-1, RANTES, TIMP-1, GRO-α, IL6, MMP-1, bNGF, FN, TGF-β1, TNF-α [37]. However, for the purposes of the current study, CCL2 and CCL5 were selected because of their critical role in the NF-κB signaling pathway. Transplanted SRC reduced presence of CCL5 in the ZSF1 model of DN. By 35 weeks of age, obese rats demonstrated more robust NF-κB activation compared with 18-week-old obese rats,

reflecting the progressive nature of DN (Figure 3A). Unlike the 5/6N$_x$ model (Figure 1A), we did not observe robust NF-κB activation in glomerular cells at early or late time points (Figure 3A). Western analysis confirmed that expression and nuclear localization of p65 increased in obese rats over time (Figure 3B). Increased NF-κB activation and interstitial inflammation were consistent observations between the surgical model (5/6N$_x$) and genetic model (obese *ZSF1*) of CKD [42,43]. As we observed that injection of SRC ameliorated chronic inflammation in the 5/6N$_x$ model, we hypothesized that these cells would prove efficacious in attenuating renal inflammation in the ZSF1 model as well. As noted in the 5/6N$_x$ study, CCL2 expression was unaltered as a result of SRC injection (Figure 4A). However, CCL5 moderately increased over time as disease state progressed and this rate was attenuated in SRC-injected animals (Figure 4B).

CM from human SRC can attenuate NF-κB activation *in vitro* independent of vesicle-mediated cell signaling. While delivery of rat SRC to chronically diseased kidneys induced long-term benefits, there is limited evidence for SRC engraftment upon implantation *in vivo* [21–23]. These observations notwithstanding, induction of a regenerative response index representing a composite protein expression biomarker reflective of stem and progenitor cell bioactivity is increased in 5/6N$_x$ model upon injection of SRC [29]. Together, these data suggest that SRC leverage indirect, paracrine mechanisms to mediate observed functional outcomes [37], consistent with other studies on MOA of cell-based therapies in acute/chronic rodent models of renal disease [44–51]. To test this hypothesis *in vitro*, CM from human SRC cultures was collected to determine the capacity for attenuating NF-κB activation as well as enhancing cellular proliferation in target cell types.

An important contribution to the transition of animal studies to clinical trials is the availability of *in vitro* assays that are predictive for an *in vivo* response. To this end, EMT of renal epithelial tubular cell populations is believed to play a significant role in the development of tubulointerstitial fibrosis during the progression of CKD [52,53]. Cytokines including TGF-β1 have been shown to recapitulate EMT within populations of tubular epithelial cells [53,54] and TGF-β1-induced EMT of the human primary tubular epithelial cell line HK2 is now a well-established model system to evaluate the impact of small molecule and protein factors on EMT [54,55]. CM derived from SRC was observed to attenuate TGF-β1-induced EMT in HK2 cells [37]. HRMC are pericytes derived from the peripheral, capillary loop-associated vasculature found within the glomerular tufts. HRMC may potentially function to establish mesangial ECM, internalization of plasma components and regulation of hormonal elements associated with control of the vasculature. Uncontrolled growth of HRMC, and therefore, of HRMC-derived mesangial matrix, may manifest in multiple aspects of glomerulonephritis, glomerulosclerosis and nephropathies. Given that synthesis of mesangial matrix by HRMC is a function of externally applied signaling factors, HRMC are commonly regarded as model platforms for fibrosis secondary to CKD [56–59]. In the current manuscript, commercially available HRMC were used as surrogates for host-response tissues in the *in vitro* assays since mesangial cells express PAI-1 in injured/diseased kidneys [25–27,56–61]. We note also that the use of TGF-β1 and TNF-α to mimic *in vitro* renal disease and treatment options is well established in the literature [56–59]. Concentration–effect curves and time-course evaluations have also been extensively reported in the literature, for an example please see [60]. Assay conditions used in the current manuscript are based on those previously established in the literature [56–60].

As a functional test of the CM in the context of kidney disease, we designed an *in vitro* assay using the human proximal tubule cell line HK2 as a surrogate for responding host cells. Nuclear shuttling of p65 was inhibited by SRC-CM (Figure 6). To identify bioactive component(s) of SRC-CM responsible for NF-κB and PAI-1 attenuation capacity, media was subjected to ultracentrifugation at 200,000 g. This vesicle-rich media was unable to attenuate NF-κB activity (Figure 8A), showing that NF-κB suppressor(s) contained within SRC-CM are not directly associated with secreted vesicles and that the bioactive component is smaller than 5 kDa. Proliferation was assayed by evaluation of the expression of the cell cycle regulators CyclinD1 and FOS, both markers of cell cycle regulation [62]. Although it remains possible that the components (<5 kDa) that induce tubular epithelial cell proliferation are the same as those which attenuate NF-κB activation, we have no data currently to confirm this point. Given the low molecular weight (<5 kDa) of the bioactive factors, it is likely that these factors are small-molecule compounds or small peptides and not proteins. However, in the absence of further data, we cannot speculate regarding the identity of these compounds. Attenuation of the TGF-β-mediated signaling pathway regulating expression of PAI-1 is associated with soluble factors contained in vesicle rich CM (Figure 9A & B). Finally, direct comparison between vesicle-rich and vesicle-depleted SRC media shows proliferation is

enhanced in target epithelia by nonvesicular factors (Figure 10). A complete cataloging of miRNAs present in SRC-CM is the subject of a future manuscript [Basu *et al.* (2016), Manuscript in Preparation]. For the sake of clarity, we have chosen to focus in the current manuscript on miRNAs directly relevant to the PAI-1/NF-κB signaling pathway for which unambiguous functional data are available. On this basis, miR-449a was selected for further functional analysis. However, other relevant miRNAs identified in the current study and their RNA targets include: miR-30b-5p (both regulators of PAI-1), miR-21 (Pellino-1), miR-146a (IRAK/TRAF6), miR-124 and miR-151 (NF-κB). As predicted, transfection of synthetic miR-449a-reduced basal and TGF-β-induced expression of PAI-1 protein (compare lane 1 with lane 3, and lanes 2 and 4, Figure 9C). In addition to its role in regulation of PAI-1, miR-449a is well established as a potent inducer of cell death, cell cycle arrest and/or cell differentiation [34].

Our earlier studies have demonstrated that SRC can be identified within the implanted kidney at up to 3 months postimplantation, albeit at reduced frequency. In the 5/6$N_x$ model leveraging male donors and female recipients, male SRC were detectable within the remnant kidney of the $N_x$ female recipient host at 4 weeks after implant, as evidenced by visualization of PKH-26 dye-labeled cells within the parenchyma adjacent to the injection site. Retention of donor cells at the 3-month time point was verified in frozen tissue sections by FISH with rat Y/12 chromosome probes, confirming the presence of male donor cells in tubular and peritubular regions, predominantly localized within the corticomedullary zone. Finally, detection of the male-specific *SRY* gene by PCR in serial tissue sections supported the Y-chromosome FISH findings, demonstrating that the majority of $SRY^+$ donor-derived DNA persisted in the cortical/corticomedullary junction zone at an estimated frequency of 1:33,333 cells. $SRY^+$ DNA was found less frequently in the medullary zone and no $SRY^+$ DNA was detected in the papillary/pelvic zone suggesting that $SRY^+$ cells are retained preferentially within the CMJ zone [22].

The ZSF1 model leveraged SRC labeled with SPIO for whole organ detection by MRI and fluorescence microscopy following intrarenal transplantation into the anterior pole of the left kidney in obese diabetic ZSF1-recipient rats. MRI revealed a region of negative contrast at the anterior pole of the kidney where the cells were injected. These data are consistent with whole organ fluorescent imaging highlighting the injection site and iron-conjugated rhodamine located at the upper cortex of the anterior pole. Sectioning of the whole kidney indicated a bolus of iron–rhodamine-labeled cells by fluorescent detection and by Prussian-blue for iron migrating and distributing from the cortical injection site, confirming their presence in tubular and peritubular spaces of the cortex and medulla. In parallel with the qualitative MRI-based cell detection study, an *in vivo* study was performed to trace ZSF1 renal cells labeled with perfluorocarbon tracer Cell Sense DM-Red 19F by NMR. The robust detection of 19F-labeled cells at 3 and 24 h following implantation confirmed their early retention in the kidney and the diminished yet significant detection of 19F 7 days following the transplantation procedure. SRC retention was consistent with the detection of these cells observed in the 5/6$N_x$ nephrectomy mass reduction model using both *SRY* gene detection and FISH for Y chromosome (male donor cell detection in female recipients), and cell-membrane PKH-26 dye-labeled studies [22, 23]. It remains unclear if continued or improved persistence of these cells would significantly improve the extent of immunomodulation.

## Conclusion

To summarize, we have demonstrated in two models of CKD that robust NF-κB activation, PAI-1 expression and subsequent inflammation and fibrosis are common pathological outcomes despite their disparate etiologies. We confirm that a SRC cell-based approach can effectively promote resolution of CKD-related etiologies through influence on NF-κB signaling pathways in both disease models. An impact on TGF-β1 signaling is also suggested by the *in vitro* data but will require additional *in vivo* confirmation. Finally, we demonstrate both *in vitro* and *in vivo* that SRC specifically promotes proliferation of target tubular epithelial cells through secreted factors and in conjunction with effects on NF-κB activation and PAI-1 expression may attenuate advancement of CKD. Unequivocal proof of the existence of microvesicles in SRC-CM will require electron microscopic confirmation; such experiments are currently in progress.

Future studies on optimization of SRC-based renal cell therapy will include systematic dose-response analysis to identify optimal SRC dosage. To this end, a comparative evaluation of low dose ($10^6$ SRC) versus high dose ($10^7$ SRC) has been made and reported in [22]. Briefly, essentially identical and statistically significant stabilization of serum creatinine and BUN was observed from transplantation of both high and low doses of SRC in the 5/6$N_x$ model, suggesting that $10^6$ SRC may be acceptable for a rodent product prototype, greatly facilitating the manufacturing process. The potential impact of donor-specific dif-

ferences on SRC potency and bioactivity has thus far not been evaluated, in part because of the absence of a noninbred rodent model for CKD. Additionally, as SRC therapy is by definition autologous, the relevance of such studies to the SRC clinical program is minimal. Taken together, these studies extend and complement previous work on SRC-related MOA demonstrating mobilization of host-derived stem and progenitor-associated markers in 5/6$N_x$ rodent models of CKD in response to treatment with SRC [29]. Identification of putative MOA(s) establishes the foundation for potency assay development and implementation, critical for successful clinical translation of any biologic product candidate [38,39]. To this end, Phase I/II clinical trials of Neo-Kidney Augment, a SRC/hydrogel composite cell therapeutic for treatment of ESRD, have been initiated [63,64].

## Future perspective

Identification of putative MOA(s) establishes the foundation for potency assay development and implementation, critical for successful clinical translation of any biologic product candidate. As we have discussed in [39,40], growth factors and miRNAs secreted by SRC may be directly incorporated into a battery of functional bioassays that taken together provide a quantitative index of product potency. The development of renal fibrosis during progressive onset of CKD may be modeled *in vitro* by the induction of an EMT event in certain populations of renal cells with TGF-β. Factors present in SRC-derived CM are capable of blocking or reversing this EMT event, which may be monitored quantitatively by PCR methods providing another index of SRC bioactivity [38, 39]. Finally, RegenMedTX LLC's Neo-Kidney Augment (NKA) is a SRC/hydrogel composite cell therapeutic currently undergoing Phase I/II clinical trials in Sweden and the USA (ClinicalTrials.gov identifier #NCT01846715 and NCT02008851) for patients with Type 2 diabetes and CKD [63, 64]. It is expected that clinical data derived from these trials will further refine our understanding of mechanistic pathways associated with SRC therapeutic bioactivity.

### Financial & competing interests disclosure

The authors declare an equity and intellectual property interest in Tengion, Inc., Assets of Tengion Inc. have since been acquired by RegenMedTX, LLC. The authors have no other relevant affiliations or financial involvement with any organization or entity with a financial interest in or financial conflict with the subject matter or materials discussed in the manuscript apart from those disclosed.

No writing assistance was utilized in the production of this manuscript.

### Ethical conduct of research

The authors state that they have obtained appropriate institutional review board approval or have followed the principles outlined in the Declaration of Helsinki for all human or animal experimental investigations. In addition, for investigations involving human subjects, informed consent has been obtained from the participants involved.

### Executive summary

**Molecular characterization of rodent chronic kidney disease models**

- Progressive NF-κB activation and interstitial inflammation are features in the development of chronic kidney disease in the 5/6 nephrectomy (5/6$N_x$) model.

**Selected renal cell mechanism of action, 5/6$N_x$ model**

- Transplanted selected renal cell (SRC) attenuate NF-κB and PAI-1 activation and reduce macrophage and T-cell infiltration in the 5/6 nephrectomy model.
- Transplanted SRC promote tubular cell proliferation in 5/6$N_x$ rats.

**SRC mechanism of action, ZSF model**

- Transplanted SRC attenuate NF-κB signaling and PAI-1 expression in ZSF1 model of diabetic nephropathy.

**Effect of SRC-derived conditioned media**

- Conditioned media (CM) from human SRC can attenuate NF-κB activation *in vitro* independent of vesicle-mediated cell signaling.

**Role of vesicular component of SRC-derived CM**

- Secreted vesicles in CM from rat and human SRC can attenuate PAI-1 expression *in vitro*; bioactivity is mediated in part by miRNAs.

**Role of nonvesicular component of SRC-derived CM:**

- Nonvesicle components of SRC-CM induce tubular cell proliferation.

**Clinical trials**

- RegenMedTX LLC's Neo-Kidney Augment is a SRC/hydrogel composite cell therapeutic currently undergoing Phase I/II clinical trials in Sweden and the USA for patients with Type 2 diabetes and chronic kidney disease.

## References


Papers of special note have been highlighted as:
• of interest; •• of considerable interest

1 U.S. Renal Data System. Costs of CKD and ESRD, Minneapolis, MN, USA (2007). www.usrds.org/2007/pdf/00_intro_07.pdf

▶2 Moudgil A, Bagga A. Evaluation and treatment of chronic renal failure. *Indian J. Pediatr.* 66, 241–253 (1999).

3 Annual Report of the U.S. Organ Procurement and Transplantation Network and the Scientific Registry of Transplant Recipients: Kidney Transplant Data 2008. Department of Health and Human Services, Health Resources and Services Administration, Healthcare Systems Bureau, Division of Transplantation, Rockville, MD; United Network for Organ Sharing, Richmond, VA; University Renal Research and Education Association, Ann Arbor, MI.

▶4 Tumlin J, Wali R, Williams W *et al.* Efficacy and safety of renal tubule cell therapy for acute renal failure. *J. Am. Soc. Nephrol.* 19, 1034–1040 (2004).

▶5 Togel F, Cohen A, Zhang P, Yang Y, Hu Z, Westenfelder C. Autologous and allogeneic marrow stromal cells are safe and effective for the treatment of acute kidney injury. *Stem Cells Dev.* 18, 475–485 (2009).

▶6 Westenfelder C. Protective actions of administered mesenchymal stem cells in acute kidney injury:relevance to clinical trials. *Kidney Int.* (Suppl. 1), 103–106 (2011).

▶7 Humphreys BD, Bonventre JV. Mesenchymal stem cells in acute kidney injury. *Annu. Rev. Med.* 59, 311–325 (2008).

▶8 Basu J, Ludlow JW. Developmental engineering the kidney: leveraging principles of morphogenesis for renal regeneration. *Birth Defects Res. C. Embryo Today* 96, 30–38 (2012).

▶9 Yokoo T, Fukui A, Ohashi T *et al.* Xenobiotic kidney organogenesis from human mesenchymal stem cells using a growing rodent embryo. *J. Am. Soc. Nephrol.* 17, 1026–1034 (2006).

▶10 Kim SS, Gwak SJ, Han J *et al.* Kidney tissue reconstruction by fetal kidney cell transplantation: effect of gestation stage of fetal kidney cells. *Stem Cells* 25, 1393–1401 (2007).

▶11 Marshall D, Dilworth MR, Clancy M, Bravery CA, Ashton N. Increasing renal mass improves survival in anephric rats following metanephros transplantation. *Exp. Physiol.* 92, 263–271 (2007).

▶12 Patschan D, Plotkin M, Goligorsky MS. Therapeutic use of stem and endothelial progenitor cells in acute renal injury: ça ira. *Curr. Opin. Pharmacol.* 6, 176–183 (2006).

▶13 Chade AR, Zhu X, Lavi R *et al.* Endothelial progenitor cells restore renal function in chronic experimental renovascular disease. *Circulation* 119, 547–557 (2009).

▶14 Prodromidi EI, Poulsom R, Jeffery R *et al.* Bone marrow-derived cells contribute to podocyte regeneration and amelioration of renal disease in a mouse model of Alport syndrome. *Stem Cells* 24, 2248–2455 (2006).

▶15 Kirpatovskii VI, Kazachenko AV, Plotnikov EY *et al.* Experimental intravenous cell therapy of acute and chronic renal failure. *Bull. Exp. Biol. Med.* 143, 160–165 (2007).

▶16 Sagrinati C, Ronconi E, Lazzeri E, Lasagni L, Romagnani P. Stem-cell approaches for kidney repair: choosing the right cells. *Trends Mol. Med.* 14, 277–285 (2008).

▶17 Basu J, Ludlow JW. Platform technologies for tubular organ regeneration. *Trends Biotechnol.* 28, 526–533 (2010).

18 Basu J, Ludlow JW. Tissue engineering of tubular and solid organs: an industry perspective. In: *Advances in Regenerative Medicine.* Wislet-Gendebien S (Ed.). InTech Open Publishers, Rijeka, Croatia (2011).

▶19 Guo JK, Cantley LG. Cellular maintenance and repair of the kidney. *Annu. Rev. Physiol.* 72, 357–376 (2010).

▶20 Lin F, Moran A, Igarashi P. Intrarenal cells, not bone marrow derived cells, are the major source for regeneration in postischemic kidney. *J. Clin. Invest.* 115, 1756–1764 (2005).

▶21 Bruce AT, Guthrie KI, Kelley R. *Ex vivo* culture and separation of functional renal cells. *Methods Mol. Biol.* 1001, 53–64 (2013).

▶22 Kelley R, Werdin ES, Bruce AT *et al.* Tubular enriched subpopulation of primary renal cells improves survival and augments kidney function in a rodent model of chronic kidney disease. *Am. J. Physiol. Renal Physiol.* 299(5), F1026–F1039 (2010).

•• **First demonstration of selected renal cell (SRC) functionality in preclinical rodent model.**

▶23 Kelley R, Bruce A, Spencer T *et al.* A population of selected renal cells augments renal function and extends survival in the ZSF1 model of progressive diabetic nephropathy. *Cell Transplant.* 22, 1023–1039 (2013).

•• **First demonstration of SRC functionality in preclinical diabetic rodent model.**

▶24 Border WA, Noble NA. Transforming growth factor beta in tissue fibrosis. *N. Engl. J. Med.* 331, 1286–1292 (1994).

▶25 Eddy AA, Fogo AB. Plasminogen activator inhibitor-1 in chronic kidney disease: evidence and mechanisms of action. *J. Am. Soc. Nephrol.* 17, 2999–3012 (2006).

▶26 Seo JY, Park J, Yu MR, Kim YS, Ha H, Lee HB. Positive feedback loop between plasminogen activator inhibitor-1 and transforming growth factor-beta1 during renal fibrosis in diabetes. *Am. J. Nephrol.* 30, 481–490 (2009).

▶27 Liu Y. Renal fibrosis: new insights into the pathogenesis and therapeutics. *Kidney Int.* 69, 213–217 (2006).

▶28 Liu BC, Zhang L, Lv LL, Wang YL, Liu DG, Zhang XL. Application of antibody array technology in the analysis of urinary cytokine profiles in patients with chronic kidney disease. *Am. J. Nephrol.* 26, 483–490 (2006).

▶29 Genheimer CW, Ilagan RM, Spencer T *et al.* Molecular characterization of the regenerative response induced by intra-renal transplantation of selected renal cell in a rodent model of chronic kidney disease. *Cells Tissues Organs* 196, 374–384 (2012).

▶30 Bilan VP, Salah EM, Bastacky S *et al.* Diabetic nephropathy and long-term treatment effects of rosiglitazone and enalapril in obese ZSF1 rats. *J. Endocrinol.* 210, 293–308 (2011).

▶31 Tofovic SP, Jackson EK. Rat models of the metabolic syndrome. *Methods Mol. Med.* 86, 29–46 (2003).

32 ImageJ. http://imagej.nih.gov/ij/

33 Mirbase. www.mirbase.org

34 Lizé M, Klimke A, Dobbelstein M. MicroRNA-449 in cell fate determination. *Cell Cycle* 10, 2874–2882 (2011).

35 Aboushwareb T, Egydio F, Straker L, Gyabaah K, Atala A, Yoo JJ. Erythropoietin producing cells for potential cell therapy. *World J. Urol.* 26, 295–300 (2008).

36 Caplan AI, Correa D. The MSC: an injury drugstore. *Cell Stem Cell* 9, 11–15 (2011).

37 Basu J, Genheimer CW, Rivera EA *et al.* Functional evaluation of primary renal cell/biomaterial neo-kidney augment prototypes for renal tissue engineering. *Cell Transplant.* 20, 1771–1790 (2011).

• **Systematic profiling of character and function of SRC.**

38 Basu J, Ludlow JW. Cell-based therapeutic products: potency assay development and application. *Regen. Med.* 9, 497–512 (2014).

•• **First clear and systematic proposal for potency assay development of clinical cell therapy products.**

39 Guthrie K, Bruce A, Sangha N, Rivera E, Basu J. Potency evaluation of tissue engineered and regenerative medicine products. *Trends Biotechnol.* 31, 505–514 (2013).

•• **First clear and systematic proposal for potency assay development of clinical tissue-engineered products.**

40 Humphreys BD. Genetic tracing of the epithelial lineage during mammalian kidney repair. *Kidney Int. Suppl.* 1(3), 83–86 (2011).

41 Humphreys BD, Valerius MT, Kobayashi A *et al.* Intrinsic epithelial cells repair the kidney after injury. *Cell Stem Cell* 2, 284–291 (2008).

•• **Demonstration of role of host-derived tubular epithelial cells for mediating kidney repair.**

42 Ninichuk V, Khandoga AG, Segerer S *et al.* The role of interstitial macrophages in nephropathy of Type 2 diabetic db/db mice. *Am. J. Pathol.* 170, 1267–1276 (2007).

43 Tapmeier TT, Fearn A, Brown K *et al.* Pivotal role of $CD4^+$ T cells in renal fibrosis following ureteric obstruction. *Kidney Int.* 78, 351–362 (2010).

44 Villanueva S, Carreño JE, Salazar L *et al.* Human mesenchymal stem cell derived from adipose tissue reduce functional and tissue damage in a rat model of chronic renal failure. *Clin. Sci.* 125, 199–210 (2013).

45 Menke J, Iwata Y, Rabacal WA *et al.* CSF1 signals directly to renal tubular epithelial cells to mediate repair in mice. *J. Clin. Invest.* 119, 2330–2342 (2009).

46 Cheng K, Rai P, Plagov A *et al.* Transplantation of bone-marrow derived MSCs improves *cis*-platinum induced renal injury through paracrine mechanisms. *Exp. Mol. Pathol.* 94, 466–473 (2013).

47 Bagul A, Frost JH, Drage M. Stem cells and their role in renal ischemia reperfusion injury. *Am. J. Nephrol.* 37, 16–29 (2013).

48 Gatti S, Bruno S, Deregibus MC *et al.* Microvesicles derived from human adult mesenchymal stem cells protect against ischemia-reperfusion induced acute and chronic kidney injury. *Nephrol. Dial. Transplant.* 26, 1474–1483 (2011).

49 Yamaleyeva LM, Guimaraes-Souza NK, Krane LS *et al.* Cell therapy with human renal cell cultures containing erythropoietin positive cells improves chronic kidney injury. *Stem Cells Transl. Med.* 1, 373–383 (2012).

50 Guimarães ET, Cruz Gda S, Almeida TF *et al.* Transplantation of stem cells obtained from murine dental pulp improves pancreatic damage, renal function and painful diabetic neuropathy in diabetic type I mouse model. *Cell Transplant.* 22(12), 2345–2354 (2012).

51 Du T, Cheng J, Zhong L *et al.* The alleviation of acute and chronic kidney injury by human Wharton's jelly-derived mesenchymal stromal cells triggered by ischemia-reperfusion injury via an endocrine mechanism. *Cytotherapy* 14, 1215–1227 (2012).

52 Humphreys BD, Lin S, Kobayashi L *et al.* Fate tracing reveals the pericyte and not epithelial origin of myofibroblasts in kidney fibrosis. *Am. J. Pathol.* 176, 85–97 (2009).

53 Okada H, Inoue T, Suzuki H, Strutz F, Neilson EG. Epithelial–mesenchymal transformation of renal tubular epithelial cells *in vitro* and *in vivo*. *Nephrol. Dial. Transplant.* 15, 44–46 (2000).

54 Dudas PL, Argentieri RL, Farrell FX. BMP-7 fails to attenuate TGF-β1-induced epithelial-to-mesenchymal transition in human proximal tubule epithelial cells. *Nephrol. Dial. Transplant.* 24, 1406–1416 (2009).

55 Hills CE, Al-Rasheed N, Willars GB, Brunskill NJ. C-peptide reverses TGF-beta1-induced changes in renal proximal tubular cells: implications for treatment of diabetic nephropathy. *Am. J. Physiol. Renal Physiol.* 296, F614–F621 (2009).

56 Rodriguez-Barbero A, L'Azou B, Cambar J, Lopez-Novoa JM. Potential use of isolated glomeruli and cultured mesangial cells as *in vitro* models to assess nephrotoxicity. *Cell Biol. Toxicol.* 16, 145–153 (2000).

57 Zeisberg M, Maeshima Y, Mosterman B, Kalluri R. Renal fibrosis. Extracellular matrix microenvironment regulates migratory behavior of activated tubular epithelial cells. *Am. J. Pathol.* 160, 2001–2008 (2001).

58 Stockand JD, Sansom SC. Regulation of filtration rate by glomerular mesangial cells in health and diabetic renal disease. *Am. J. Kidney Dis.* 29, 971–981 (1977).

59 Grond J, Weening JJ. Mesangial cell injury, glomerulosclerosis, and therapeutic intervention. *Contrib. Nephrol.* 81, 229–239 (1990).

60 Kanalas JJ, Hopfer U. Effect of TGF-beta 1 and TNF-alpha on the plasminogen system of rat proximal tubular epithelial cells. *J. Am. Soc. Nephrol.* 8, 184–192 (1997).

61 Rerolle JP, Hertig A, Nguyen G *et al.* Plasminogen activator inhibitor type 1 is a potential target in renal fibrosis. *Kidney Int.* 58, 1841–1850 (2000).

62 Brown JR, Nigh E, Lee RJ *et al.* Fos family members induce cell cycle entry by activating cyclin D1. *Mol. Cell. Biol.* 18, 5609–5619 (1998).

63 Clinical trials database. http://clinicaltrials.gov/ct2/show/NCT01846715

64 Clinical trials database. http://clinicaltrials.gov/ct2/show/NCT02008851